Auton Robot (2009) 26: 47–78
DOI 10.1007/s10514-008-9106-7

Asymmetric trajectory generation and impedance control for running of biped robots

Ohung Kwon · Jong Hyeon Park

Received: 19 July 2007 / Accepted: 15 October 2008 / Published online: 28 October 2008

Abstract An online asymmetric trajectory generation method for biped robots is proposed to maintain dynamical postural stability and increase energy autonomy, based on the running stability criterion defined in phases. In a support phase, an asymmetric trajectories for the hip and swing leg of the biped robots is obtained from an approximated running model with two springless legs and a spring-loaded inverted pendulum model so that the zero moment point should exist inside the safety boundary of a supporting foot, and the supporting leg should absorb large reaction forces, take off and fly through the air. The biped robot is under-actuated with six degrees of under-actuation during flight. The trajectory generation strategies for the hip and both legs in a flight phase use the approximated running model and non-holonomic constraints based on the linear and angular momenta at the mass center. Next, we present an impedance control with a force modulation strategy to guarantee a stable landing on the ground and simultaneously track the desired trajectories where the desired impedance at the hip link and both legs is specified. A series of computer simulations for two different types of biped robots show that the proposed running trajectory and impedance control method satisfy the two conditions for running stability and make the biped robot more robust to variations in the desired running speed, gait transitions between walking and running, and parametric modeling errors. We have examined the feasibility of this method with running experiments on a 12-DOF biped robot without arms. The biped robot could run successfully with average forward speed of about 0.3359 [m/s].

Keywords Biped robot · Running stability · Angular momentum · Asymmetric trajectory · Impedance control

1 Introduction

There is an increasing need for robots to work together and more closely with human beings. Since human beings mostly stay in artificial spaces created only for themselves, robots working in the same space as humans should have the capability to adapt themselves to artificial environments. Many artificial elements including stairs and door thresholds are hazards to robots that move around on wheels. However, such elements can be successfully and easily dealt with by biped robots that move more similarly to humans.

Most research on biped robots aims at developing design and control methods for various motion patterns closer to human-like movement. Above all, with the need for more dynamic and rapid motions, it is important for biped robots to have capabilities like running naturally. Progress in this direction has many difficulties since biped robots are mechanical systems with a changing number of degrees of freedom (e.g. due to contact) and under-actuated mechanisms with non-holonomic constraints. In addition, the control system responsible for various maneuvers must also take action in anticipation of the ballistic phase, in that linear and angular momentum cannot be manipulated once the ballistic phase begins (Frohlich 1979).

Electronic supplementary material The online version of this article (http://dx.doi.org/10.1007/s10514-008-9106-7) contains supplementary material, which is available to authorized users.

O. Kwon
Department of Mechanical Engineering, Hanyang University, Seoul, Korea
e-mail: ohung210@hanyang.ac.kr

J.H. Park (✉)
School of Mechanical Engineering, Hanyang University, Seoul, Korea
e-mail: jongpark@hanyang.ac.kr

Despite these difficulties, Raibert and colleagues first have studied hopping and running robots (Raibert 1986; Hodgins and Raibert 1991; Hodgins 1991; Playter and Raibert 1992). They built and controlled a series of multi-legged machines beginning with an one-legged machine driven by pneumatic and hydraulic actuators using the decoupled control algorithms and their machines performed various actions including running up and down on the stairs and somersaults. After their work, these types of robots which are equipped with a spring mechanism to restore kinetic energy during a stance phase have been widely studied (Lapshin 1991; Ahmadi and Buehler 1997; Francois and Samson 1998; Hyon and Emura 2004). With their elegant mechanical models with compliant elements, complex dynamical behaviors were achieved by control algorithms which guarantee the existence of the Poincaré return map associated with periodic running gaits and their stability properties for a running legged robot.

Such stable and energy-efficient control methods have been applied for various legged robots with revolute joints and no leg spring to move with symmetry at touch-down and take-off using a spring-loaded inverted pendulum model (SLIP model) (Saranli et al. 1998). In multi-body legged robots where the total center of mass is not located at the hip joint, it is difficult to calculate the exact flight and stance trajectories because it requires the explicit solution to the robot's equations of motion. Inaccurate knowledge leads to rapid failure of dynamic running due to under-actuation and non-holonomic constraint caused by the conservation of angular momentum in flight. For stable dynamic running, Chevalereau et al. developed asymptotically stable running gaits using a hybrid zero dynamics for running of a planar biped robot with revolute joints, designed without feet (Chevalereau et al. 2005). To minimize the effect of unmodeled dynamics, Ikeda et al. proposed a control strategy of legged robots which realizes differential equations as controlled constraints, i.e., time responses of the position of the center of mass of the whole robot, the zero angular momentum about the center of mass, and the angular momentum with respect to the toe which are obtained from the photograph data of the gait motion of a kangaroo (Ikeda et al. 1999). Kajita et al. proposed methods to generate running trajectories for a humanoid robot using linear and angular momentum equations of considerable complexity (Kajita et al. 2002, 2004). The highly successful control concepts for walking gaits of biped robots have been expanded into dynamic running using constraints that the ZMP is within the safety polygon in the support phase and the angular momentum about the center of mass is almost zero or inside the limited range in the flight phase (Park and Kwon 2003; Kwon and Park 2003; Nagasaka et al. 2004).

In our previous studies, to control effectively the under-actuated mechanical system with a changing number of degrees of freedom, the following conditions were addressed: 1) A full running cycle is divided into a support phase and a flight phase, 2) Non-holonomic constraints are derived by applying the linear and angular momentum theorem to the entire robot, and 3) Two legs and body form approximately symmetric configurations with respect to a vertical axis passing through the hip during the flight phase or stance phase. The analysis of running based on these conditions gives us an effective symmetric running trajectory for dealing with a biped robot without requiring detailed solutions to complex formulations (Park and Kwon 2003; Kwon and Park 2003). However, the control system requires online trajectory modification and additional forces and torques for periodic or recursive running because two heavy legs and arms may not be equally spaced about the center of mass, and foot slipping, joint friction, and modeling errors exist in the system, so that the biped robot will not perform more than a few hops. The locomotion pattern also deviates from symmetry when the control system purposely changes running speed and transits gaits.

This paper proposes an asymmetric running trajectory which is specified at the hip link and both legs of a biped robot using an approximated running model with two springless legs the mass of which is concentrated at its middle position. In the flight phase, in order for a biped robot to touch its foot on the ground exactly after the planed duration of flight and to rotate about its center of mass through the planed angle, the trajectories of the hip link and both legs are obtained from the running model and the modified linear and angular momentum equations. In running of most animals, the angular momentum about the center of mass becomes negative inside the limited range at the beginning of the touch-down and recovers to certain values, i.e., almost zero, before lift-off (Frohlich 1979; Ikeda et al. 1999; Arikawa and Mita 2002). If the angular momentum about the center of mass does not recover to the value at the beginning of the flight phase, the steady-state ballistic motions cannot be achieved. The support phase motions determine the necessary magnitude of angular momentum for the following flight phase. It is well-established that the arm and leg motions according to styles or patterns of flight require specific and significantly different amounts of angular momentum in order to produce acceptable configurations at touch-down (Ramey 1973). If the angular momentum produced at lift-off is not properly matched or inappropriate to one style of flight, the arm and leg motions according to the style of flight may result in unstable configurations at touch-down. Instead of finding the correct amount of angular momentum required for the style of flight, the leg motions during flight are determined by the angular momentum which is defined at the running model's center of mass based on the desired support phase trajectories of the hip link and two legs.

In the support phase, many of the essential characteristics of the elastic element which stores and releases energy

in the legs of a human can be captured with a SLIP model. This model has not only been used to describe and predict human locomotion, but also to move the leg of a biped robot like a linear spring (Alexander 1990; Seyfarth et al. 2002; Papadopoulos and Cherouvim 2004). Such SLIP-like (ball-like) leg motions which are achieved by elastic operation of a classical electrical drive in each leg joint of the biped robot are important for biped robots to reduce the energy consumption and achieve the stability, and facilitates control. In order to achieve the SLIP-like motion simultaneously with maintenance of stable running according to the robot's states at touch-down and lift-off, an asymmetric trajectory is generated from the approximated running model so that the biped robot bounces like a bouncing elastic ball during the support phase. The asymmetric trajectories of the hip link and two legs can be modified online according to the position and velocity of the hip link at touch-down, gait transitions and variations in the limited range of the forward running speed. Energy dissipated by the asymmetric behavior is mainly dependent on locomotion parameters (leg stiffness, hip height, and running speed), which of optimum selection makes the biped robot run with the least energy consumption. A comparison with the total energy indicates that the asymmetric motion reduces almost the same energy consumption as the SLIP-like motion.

Damage to a biped robot with mechanical gears and electrical motors caused by large external forces could be costly. Hence it is very important to reduce the external forces by managing the position and force between robot and environment. In typical human running, the leg muscles are repeatedly hardened and relaxed to regulate and reduce large impact, make a supporting leg rebound into the air and move into the proper position according to movement commands (McMahon 1984). Foot rotation or leg retraction strategies have been studied in a similar manner so that biped robots land on the ground without any damage (Kajita et al. 2005; Nunez and Nadjar-Gauthier 2005). The same control property or role is found in the impedance control that has been successfully used for robot manipulators or waking robots in frequent contact with the ground (Lewis et al. 1993; Park 2001). For stable running, an impedance control method with a force modulation strategy is proposed to comply with the external environment repeatedly and track the desired trajectories. The force modulation strategy is used to reduce drastically the magnitude of external forces exerted on the foot, since the contact force occurs about two or three times as large as the total weight of the robot, and may cause vital damage to the joints and result in a fall. The parameters in the desired impedance model are determined depending on the mechanical properties of the original system so that the gravity potential and kinetic energies are stored and transformed naturally as the limbs move.

The main contribution of this paper is an online trajectory generation method for asymmetrical behaviors and an impedance control method for stable dynamic running of biped robots with relatively heavy legs, the mass of which is homogeneously distributed, based on the defined running stability. The proper value of angular momentum for flight can be found easily according to the desired patterns of the support phase. We also present the results of experiments that explore use of impedance control in conjunction with the asymmetric trajectory by a 12-DOF biped robot. The method we propose here is a realistic, available method that does not exceed the limits of commercial actuators (e.g. permanent magnet DC motors in series with a gear train) by putting bounds to both joint torque and angular velocity. It should be noted that this paper is not concerned with the trajectory generation of biped robots with heavy links, the mass of which is asymmetrically distributed, although it is a research topic in bipedal running.

Sections 2 and 3 describe the dynamics and linear and angular momentum equations of a biped robot, and the stability criterion for stable running, respectively. Sections 4 and 5 describe the asymmetric trajectory generation method and the impedance control strategy, respectively. The effectiveness and performance of the proposed running trajectory and impedance control through a series of computer simulations and experiments are shown in Sect. 6 and Sect. 7, followed by conclusions in Sect. 8.

2 Modeling of a biped robot

Running biped robots are different from typical robot manipulators in that they do not have fixed contact points with the ground and the constraints between both feet and the ground change repeatedly as they walk and run, as shown in Fig. 1. The motion equations of a running biped robot represented by the absolute coordinates, O–XYZ, are described by the following equations (Walker and Orin 1982; Oh and Orin 1986; Fujimoto and Kawamura 1998; Park and Kim 1998):

$$\begin{bmatrix} \vec{\tau}_r \\ \vec{\tau}_l \\ \vec{\tau}_b \\ 0 \end{bmatrix} = \begin{bmatrix} H_r & 0 & 0 & K_r \\ 0 & H_l & 0 & K_l \\ 0 & 0 & H_b & K_b \\ Q_r & Q_l & Q_b & R \end{bmatrix} \begin{bmatrix} \ddot{\vec{q}}_r \\ \ddot{\vec{q}}_l \\ \ddot{\vec{q}}_b \\ \ddot{\vec{x}}_h \end{bmatrix} + \begin{bmatrix} D_r & 0 \\ 0 & D_l \\ 0 & 0 \\ P_r & P_l \end{bmatrix} \begin{bmatrix} \vec{f}_r \\ \vec{f}_l \end{bmatrix} + \begin{bmatrix} L_r \\ L_l \\ L_b \\ S \end{bmatrix} \tag{1}$$

where vectors $\ddot{\vec{q}}_r, \ddot{\vec{q}}_l \in \Re^{\rho}$, $\ddot{\vec{q}}_b \in \Re^{\varrho}$ and $\ddot{\vec{x}}_h \in \Re^6$ are the joint acceleration of the right and left legs, the joint acceleration of the upper body, and the acceleration of the hip link, and vectors $\vec{f}_r, \vec{f}_l \in \Re^6$ are the external force/moment applied at the right and left feet, respectively.

The linear momentum $\vec{P}_0$ and angular momentum $\vec{H}_0$ of the biped robot represented by the absolute coordinates are described by

$$\vec{P}_0 = \sum_{k=1}^{n} m_k \dot{\vec{r}}_{gk},$$
$$\vec{H}_0 = \sum_{k=1}^{n} (\vec{r}_{gk} \times m_k \dot{\vec{r}}_{gk} + I_{gk}\vec{\omega}_{gk}) \tag{2}$$

where $\vec{r}_{gk} = [x_k \ y_k \ z_k]^T$ denotes the position vector from the origin of the absolute coordinates to the mass center coordinates of k-th link. In general, the linear and angular momenta of the robot system about any point are not conserved since the external forces and moments may arise from gravitational force, ground contact forces, and unexpected disturbances. Transforming (2) into specific momentum equations with respect to the mass center coordinates, the components $((\vec{P}_G)_x, (\vec{P}_G)_y, (\vec{P}_G)_z)$ of linear momentum $\vec{P}_G$ and the components $((\vec{H}_G)_x, (\vec{H}_G)_y, (\vec{H}_G)_z)$ of angular momentum $\vec{H}_G$ in the frontal, sagittal, and horizontal planes can be written by the following equations:

$$\vec{P}_G = \begin{bmatrix} (\vec{P}_G)_x \\ (\vec{P}_G)_y \\ (\vec{P}_G)_z \end{bmatrix} = \begin{bmatrix} \sum_{k=1}^{n} m_k \dot{x}_k \\ \sum_{k=1}^{n} m_k \dot{y}_k \\ \sum_{k=1}^{n} m_k \dot{z}_k \end{bmatrix}, \tag{3}$$

$$\vec{H}_G = \begin{bmatrix} (\vec{H}_G)_x \\ (\vec{H}_G)_y \\ (\vec{H}_G)_z \end{bmatrix} = \begin{bmatrix} \sum_{k=1}^{n} m_k\{(y_k - Y_g)(\dot{z}_k - \dot{Z}_g) - (z_k - Z_g)(\dot{y}_k - \dot{Y}_g)\} + \sum_{k=1}^{n} J_{kx}\dot{\phi}_{kx} \\ \sum_{k=1}^{n} m_k\{(z_k - Z_g)(\dot{x}_k - \dot{X}_g) - (x_k - X_g)(\dot{z}_k - \dot{Z}_g)\} + \sum_{+}^{n} k = 1 J_{ky}\dot{\phi}_{ky} \\ \sum_{k=1}^{n} m_k\{(x_k - X_g)(\dot{y}_k - \dot{Y}_g) - (y_k - Y_g)(\dot{x}_k - \dot{X}_g)\} + \sum_{k=1}^{n} J_{kz}\dot{\phi}_{kz} \end{bmatrix} \tag{4}$$

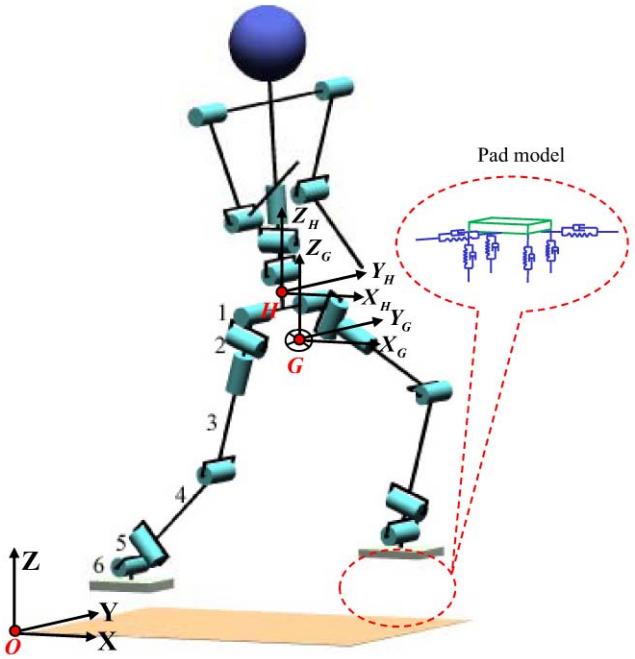

Fig. 1 Configuration of a biped robot model and its coordinate systems used for analysis and simulations. O–XYZ: Absolute coordinates, H–$X_H Y_H Z_H$: Body center coordinates fixed at the body of the robot, G–$X_G Y_G Z_G$: Mass center coordinates fixed at the mass center of the robot. The biped robot is equipped with a shock-absorbing elastic pad at its sole. The pad between the sole and the support surface is modeled as a nonlinear compliant contact model that consists of nonlinear springs with nonlinear damping. The reaction forces and moments generated at the foot in contact with the ground are computed by the amount of the pad deformation in computer simulations. When the pad is compressed, the stiffness and damping coefficient are 1.0×10^4 [N/m] and 80.0 [Ns/m], respectively. The pad has nonlinear stiffness and damping as it is compressed

where

$$X_g = \sum_{k=1}^{n} m_k x_k / m_g, \qquad Y_g = \sum_{k=1}^{n} m_k y_k / m_g,$$
$$Z_g = \sum_{k=1}^{n} m_k z_k / m_g,$$

and vector $\vec{r}_k = [x_k \ y_k \ z_k]^T$ denotes position vector of k-th link with mass m_k of the n-link biped robot. Inertias J_{kx}, J_{ky}, and J_{kz} denotes the inertia moments of k-th link represented by the mass center coordinates in the X-axis, Y-axis, and Z-axis, respectively, and $\dot{\phi}_{kx}$, $\dot{\phi}_{ky}$, and $\dot{\phi}_{kz}$ denotes the angular velocity of k-th link represented by the mass center coordinates in the X-axis, Y-axis, and Z-axis directions, respectively. The three robot body planes are used to define robot segment movements. Thus, the sagittal plane (Z–X plane) divides the robot body into symmetrical right and left halves, the frontal plane (Y–Z plane) is the vertical plane at right-angles to the sagittal plane, which divides the robot body into front and back sections, and the horizontal plane (X–Y plane) is the vertical plane at right-angles to both the sagittal plane and the frontal plane.

Basically, walking and running differ in the oscillations of the body and both legs that occur during each step or stride (Cavagna et al. 1976; Thorstensson and Roberthson 1987). These differences considered, the phases of a running cycle are divided into a support phase (or a stance phase) and a flight phase. The support phase begins at the touchdown of a freely swinging foot and ends in the lift-off of the

supporting foot, and the flight phase begins when the external force/moment applied at the right and left feet are zero and both feet are in the air. These phases are separated by two instantaneous transitions, i.e., touch-down and lift-off. The instance of touch-down indicates the moment the foot makes contact with the ground while the instance of lift-off indicates the moment the foot loses contact with the ground. The hip link (or base link) denotes the body center coordinate system that moves with the biped robot.

3 Dynamic postural stability for running

We define the running stability as the criterion of the stability evaluation for running biped robots.

Definition The running motion for biped robots is said to be *stable* if the following conditions are satisfied: The first condition is the ZMP (Zero Moment Point) condition that the ZMP should exist inside the convex hull of the foot-support in a support phase. The second condition is the angular momentum condition that the angular momentum at the mass center of the robot in a flight phase must be in a limited range.

Both conditions are discussed in detail in the next subsection.

3.1 Support phase

The ZMP concept has been used to evaluate the dynamic walking stability (Vukobratovic and Juricic 1969). If the ZMP is inside the contact polygon of the foot on the ground, the biped robot is said to be stable. Similarly, in order for running biped robots to run stably, the ZMPs in Appendix A must be within the safety boundary area so that the biped robot should land on and then take off the ground.

3.2 Flight phase

The dynamic equations of a biped robot shown in Fig. 1 can be written as follows:

$$\sum_{k=1}^{n} m_k \ddot{\vec{r}}_k = \sum_{k=1}^{n} m_k \vec{g}, \tag{5}$$

$$\sum_{k=1}^{n} \dot{\vec{H}}_{Ok} = \sum_{k=1}^{n} \vec{r}_k \times m_k \vec{g} = \sum_{k=1}^{n} \dot{\vec{H}}_{Gk} + \sum_{k=1}^{n} \vec{r}_k \times m_k \ddot{\vec{r}}_k \tag{6}$$

where vectors $\dot{\vec{H}}_{Ok}$ and $\dot{\vec{H}}_{Gk}$ denote the rates of change in angular momentum of k-th link represented by the absolute coordinates and the mass center coordinates of the biped robot, respectively; vectors $\ddot{\vec{r}}_k$ and $\vec{g} = [0\ 0\ -g]^T$ denote the acceleration of the center of mass of k-th link represented by the absolute coordinates and the gravitational acceleration, respectively. Equation (5) states that the behavior of the biped robot obeys the linear momentum after lift-off.

Rearranging (6) with respect to $\dot{\vec{H}}_{Gk}$ leads to

$$\begin{aligned}\sum_{k=1}^{n} \dot{\vec{H}}_{Gk} &= \sum_{k=1}^{n} \vec{r}_k \times m_k \vec{g} - \sum_{k=1}^{n} \vec{r}_k \times m_k \ddot{\vec{r}}_k \\ &= \sum_{k=1}^{n} \vec{r}_g \times m_k \vec{g} + \sum_{k=1}^{n} \vec{GG}_k \times m_k \vec{g} \\ &\quad - \sum_{k=1}^{n} \vec{r}_g \times m_k \ddot{\vec{r}}_k - \sum_{k=1}^{n} \vec{GG}_k \times m_k \ddot{\vec{r}}_k \end{aligned} \tag{7}$$

where $\vec{r}_k = \vec{r}_g + \vec{GG}_k$. Inserting (5) and $\dot{\vec{H}}_G = \sum_{k=1}^{n} \dot{\vec{H}}_{Gk} + \sum_{k=1}^{n} \vec{GG}_k \times m_k \ddot{\vec{r}}_k$ into (7) results in

$$\dot{\vec{H}}_G = \vec{0} \tag{8}$$

where $\dot{\vec{H}}_G$ denotes the rate of change in angular momentum at the mass center of the biped robot and vector $\vec{GG}_k$ denotes the position vector of k-th link represented by the mass center coordinates. Equation (8) states that if external forces don't act on a system of biped robot during the flight phase, the angular momentum about the center of mass is conserved and also governs a ballistic (flight) phase. The conservation law of angular momentum during the ballistic phase says,

$$\vec{H}_G = \vec{\Gamma} \tag{9}$$

where vector $\vec{\Gamma}$ is constant during the flight phase and must be in a limited range at lift-off in order to make a biped robot fly stably in the air and to satisfy the ZMP condition of the running stability when the biped robot lands on the ground.

Proof For a biped robot not to start falling down, the ZMP should remain inside the convex hull of the supporting foot in the single support phase. Equation (54) states that the x-component of the ZMP (X_{zmp}) is independent of the motion along the Y-axis. Similarly the y-component of the ZMP (Y_{zmp}) is independent of the motion along the X-axis. First, the x-component of the ZMP (X_{zmp}) must be in between $-l_h$ and l_t in the sagittal plane (Z–X plane). Thus,

$$-l_h \le X_{\text{zmp}} \le l_t \tag{10}$$

where $l_h (> 0)$ denotes the length from the center of the supporting foot to the rear safety boundary while $l_t (> 0)$ denotes the length from the center of the supporting foot to the fore safety boundary, as shown in Fig. 2. □

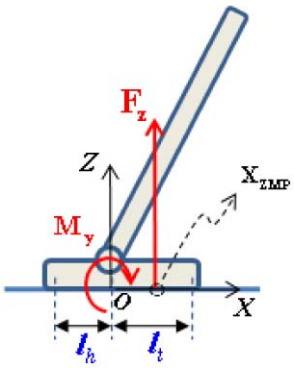

Fig. 2 Front and back boundaries of the x-component of the ZMP. The front bound l_t is a distance from the center of the support foot to the fore edge while the back bound l_h is a distance from the center of the support foot to the rear edge. F_z and M_y denote a resultant vertical force and a moment about Y-axis acting on the foot, respectively. The ZMP along X-axis is described as $X_{\text{zmp}} = -M_y/F_z$. The length and width of the foot are 0.21 [m] and 0.15 [m], respectively. $l_t = 0.134$ [m] and $l_h = 0.076$ [m] are used in the simulations and experiments

Inserting (54) into (10) leads to the following inequality with respect to the range of the rate of change in angular momentum.

$$-l_h m_g(\ddot{Z}_g + g) \le -(\dot{\vec{H}}_0)_y + \sum_{k=1}^{n} m_k g x_k \le l_t m_g(\ddot{Z}_g + g). \tag{11}$$

Substituting $(\dot{\vec{H}}_G)_y + m_g(Z_g\ddot{X}_g - X_g\ddot{Z}_g)$ for $(\dot{\vec{H}}_0)_y$ of (11) leads to

$$\begin{aligned} &-l_t m_g(\ddot{Z}_g + g) + \sum_{k=1}^{n} m_k g x_k - m_g(Z_g\ddot{X}_g - X_g\ddot{Z}_g) \\ &\le (\dot{\vec{H}}_G)_y \\ &\le l_h m_g(\ddot{Z}_g + g) + \sum_{k=1}^{n} m_k g x_k - m_g(Z_g\ddot{X}_g - X_g\ddot{Z}_g). \end{aligned} \tag{12}$$

It is assumed that the robot's configuration remains unchanged after impact due to the inelastic impulsive impact with the ground, the dynamic coupling effects between three planar motions, i.e., motions in the sagittal plane, frontal plane, and horizontal plane, is small and $(\dot{\vec{H}}_G)_{y,td}$ is equal to $((\vec{H}_G)_{y,td+} - (\vec{H}_G)_{y,td-})/\Delta t$ at small time Δt $(= t_{td+} - t_{td-} \ll 1)$ when a biped robot switches from the flight phase to the support phase. $(\vec{H}_G)_{y,td+}$ denotes the angular momentum at the moment $t = t_{td+}$ after the swing foot touches the ground while $(\vec{H}_G)_{y,td-}$ indicates the angular momentum at the moment $t = t_{td-}$ before the swing foot touches the ground. Substituting $((\vec{H}_G)_{y,td+} - (\vec{H}_G)_{y,td-})/\Delta t$ for $(\dot{\vec{H}}_G)_{y,td}$ of (12) yields

$$\begin{aligned} &-l_h m_g(\ddot{Z}_g + g)\Delta t + (\vec{H}_G)_{y,td+} \\ &\quad - \sum_{k=1}^{n} m_k g x_k \Delta t + m_G(Z_g\ddot{X}_g - X_g\ddot{Z}_g)\Delta t \\ &\le (\vec{H}_G)_{y,td-} \\ &\le (\vec{H}_G)_{y,td+} + l_t m_g(\ddot{Z}_g + g)\Delta t \\ &\quad - \sum_{k=1}^{n} m_k g x_k \Delta t + m_g(Z_g\ddot{X}_g - X_g\ddot{Z}_g)\Delta t. \end{aligned} \tag{13}$$

In general, a biped robot is controlled in order not to rotate around its center of mass during the support phase. Furthermore its center of mass (or base link) is controlled to move along the X-axis and Z-axis within a restricted speed in a predetermined distance, as given in Appendices B and C. Thus, $\|(\vec{H}_G)_{y,td+}\| \simeq \|(\vec{H}_0)_y - m_g(Z_g\dot{X}_g - X_g\dot{Z}_g)\| < \alpha_0$, $\|\ddot{Z}_g\| < \alpha_1$, and $m_g(Z_g\ddot{X}_g - X_g\ddot{Z}_g) \simeq \sum_{k=1}^{n} m_k g x_k$ $(= m_g g X_g)$ in (4) and (56). Inserting these equations into (13) leads to

$$-\alpha_2 \le (\vec{H}_G)_{y,td-} \le \alpha_3, \tag{14}$$

where α_0, α_1, α_2, and α_3 are positive values which are determined by the support phase trajectories for the biped robot. This inequality, (14), states that $(\vec{H}_G)_y$ about the center of mass during the flight phase must be within a limited range. In particular, to make the biped robot run without rotating about its center of mass in the air, the magnitude of the angular momentum must be determined to be zero before the ballistic phase begins according to the desired trajectory since the angular momentum cannot be manipulated once the flight phase begins (Frohlich 1979).

Similarly, $(\vec{H}_G)_x$ about the center of mass in the frontal plane (Y–Z plane) must be inside a limited range. $(\dot{\vec{H}}_0)_z$ in (55) will be given as

$$(\dot{\vec{H}}_0)_z = X_{\text{zmp}}F_y - F_x Y_{\text{zmp}} = m_g(X_{\text{zmp}}\ddot{Y}_g - Y_{\text{zmp}}\ddot{X}_g). \tag{15}$$

Substituting $(\dot{\vec{H}}_G)_z + m_g(X_g\ddot{Y}_g - Y_g\ddot{X}_g)$ for $(\dot{\vec{H}}_0)_z$ of (15) leads to

$$(\dot{\vec{H}}_G)_z = m_g(X_{\text{zmp}}\ddot{Y}_g - Y_{\text{zmp}}\ddot{X}_g) - m_g(X_g\ddot{Y}_g - Y_g\ddot{X}_g). \tag{16}$$

When a biped robot switches from the flight phase to the support phase, substituting $((\vec{H}_G)_{z,td+} - (\vec{H}_G)_{z,td-})/\Delta t$ for $(\dot{\vec{H}}_G)_z$ of (16) leads to

$$\begin{aligned} (\vec{H}_G)_{z,td-} = (\vec{H}_G)_{z,td+} &- m_g[(X_{\text{zmp}} - X_g)\ddot{Y}_g \\ &- (Y_{\text{zmp}} - Y_g)\ddot{X}_g]\Delta t \end{aligned} \tag{17}$$

where $\|m_g[(X_{\text{zmp}} - X_g)\ddot{Y}_g - (Y_{\text{zmp}} - Y_g)\ddot{X}_g]\Delta t\| < \beta_1$ and $\|(\vec{H}_G)_{z,td+}\| < \beta_2$, since a biped robot is controlled to follow a running trajectory within a restricted speed in a predetermined distance during the support phase, as given in Appendices B and C. β_1 and β_2 are positive values which is determined by the support phase trajectory. This inequality, (17), states that $(\vec{H}_G)_z$ must exist within a limited range.

4 Trajectory generation for running

In this section, we explore an asymmetric running trajectory for a biped robot with relatively heavy legs, based on the defined running stability criterion. The running trajectories are specified with respect to the hip link and both feet in the support and flight phases. It is assumed that a running motion can be decomposed into two planar motions, i.e., motions in the sagittal plane and the frontal plane. The robot system is an under-actuated mechanism with six degrees of under-actuation during flight. Due to the ballistic motion, six non-holonomic constraints acting on the generalized coordinates of the robot system can be derived by applying both the linear momentum theorem and the angular momentum theorem to the entire robot. The flight phase trajectories of the hip link and two legs are determined by the approximation of the non-holonomic constraints and the running model with two springless legs the mass of which is concentrated at its middle position. There will be inevitably small deviations between real trajectories and reference trajectories during the flight phase. They cause the robot to land at the wrong instance and at the wrong place, and disturb the steady running patterns for the following support phase. Such deviations require online adaptive motions of the upper body, two arms and two legs during the support phase such that at the end of that support phase the necessary initial conditions for the following flight phase are reached. The online adaptive motions are achieved by asymmetric behaviors of the hip link and two legs based on the SLIP-like motion that reduces the energy consumption.

It is assumed that a collision between foot and ground occurs inelastically, so that the foot after touch-down remains unchanged on the ground. Actually, the contacting foot may bounce back from the ground. Such a problem is considered in the impedance control with a force modulation strategy. Arm action is compensatory and synchronous with the action of the legs in order to compensate the yaw moment generated by the swing motions of two legs and the upper body remains leaned a little toward the vertical axis in order not to rotate about an axis along a line going through its center of mass.

4.1 Flight phase trajectories

The behavior of a biped robot obeys linear and angular momenta after lift-off as shown in (5) and (8), assuming that no external forces act on the system during the flight phase. Translational motion of the robot's center of mass governed by the linear momentum describes a parabola even though joint actuators are driven. The parabola depends only on the position and velocity of the center of mass at lift-off. Thus, the biped robot moves entirely under the action of gravity like a projectile moving through space, once it takes off the ground. Rotational motion around the robot's center of mass is governed by the angular momentum, which is kept constant even though each joint actuator is driven. The magnitude of the angular momentum at the center of mass during the flight phase depends on the position and velocity of all links with mass distribution, i.e., two legs, upper body and two arms.

We explore an asymmetric trajectory of the upper body and relatively heavy legs for a biped robot during flight. After determining an asymmetric motion of the hip link, the leg trajectories are determined by the modified linear and angular momentum equations with respect to the center of mass. In order for a biped robot to contact on the ground exactly after the predetermined duration of flight and to rotate about its center of mass through the planed angle, the trajectories of the hip link and two legs are obtained from an approximated running robot model with no leg spring, which is composed of two links, one for the front leg and the other for the hind leg, as shown in Fig. 3. The total mass M of the trunk and upper parts of the robot is lumped at the hip link, but the masses M_1 and M_2 are concentrated at the middle of the left leg and right leg, respectively. The period of a flight phase is divided into three breakpoints: configuration A at the beginning, configuration B in the middle, and configuration C at the end of a flight phase. The configuration A denotes the moment the robot lifts off, configuration B the moment the robot reaches to the highest flight height, and configuration C the moment the front foot strikes the ground. The essential characteristics of the ballistic motion can be captured with the three breakpoints which are used to reduce the computation time.

The modified components $(\vec{P}'_G)_x$, $(\vec{P}'_G)_y$, $(\vec{P}'_G)_z$ of the linear momentum in (3) with respect to the position and velocity of the hip link (X_j, Y_j, Z_j) and two feet (X_{ij}, Y_{ij}, Z_{ij}) at each configuration are described by the following equations:

$$
\begin{aligned}
(\vec{P}'_G)_x &= m_g \dot{\overline{X}}_j = (M + M_1/2 + M_2/2)\dot{X}_j + M_1\dot{X}_{1j}/2 \\
&\quad + M_2\dot{X}_{2j}/2 \\
(\vec{P}'_G)_y &= m_g \dot{\overline{Y}}_j = (M + M_1/2 + M_2/2)\dot{Y}_j + M_1\dot{Y}_{1j}/2 \\
&\quad + M_2\dot{Y}_{2j}/2 \\
(\vec{P}'_G)_z &= m_g \dot{\overline{Z}}_j - m_g g T_f (r-1)/2 \\
&= (M + M_1/2 + M_2/2)\dot{Z}_j + M_1\dot{Z}_{1j}/2
\end{aligned}
$$

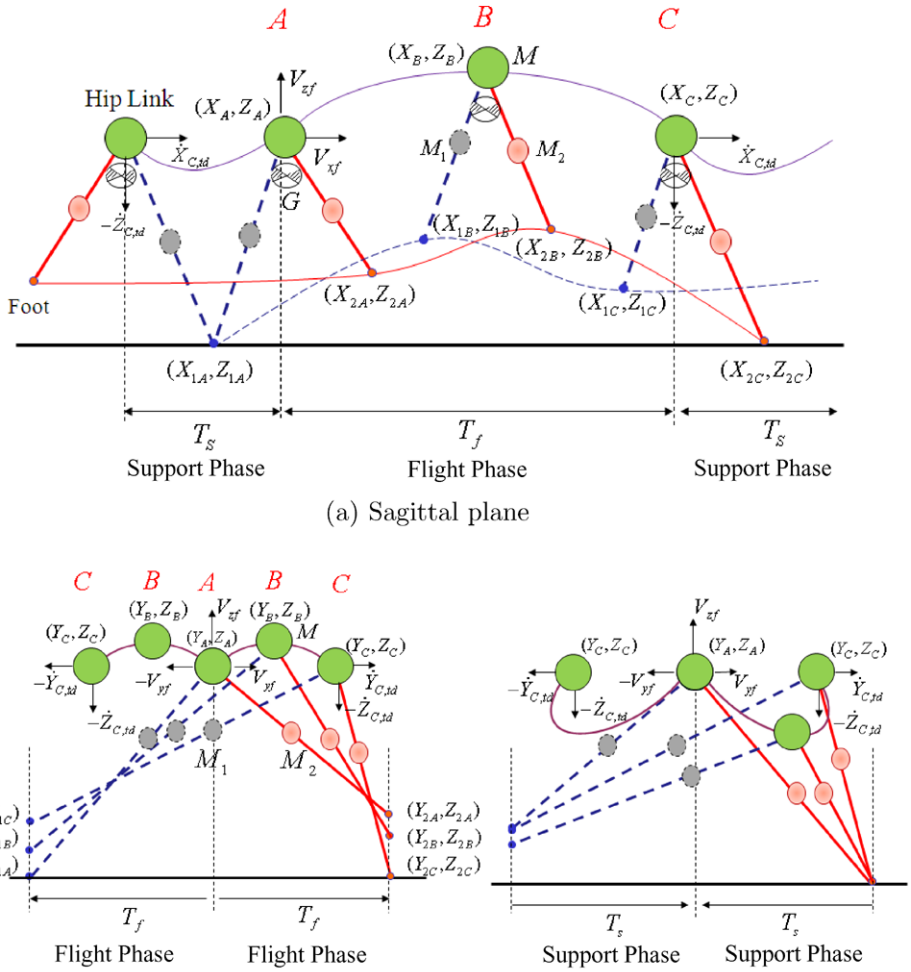

Fig. 3 An approximated running model with two legs in the sagittal and frontal planes is embedded into a biped robot with relatively heavy legs. The mass of each leg is assumed to be concentrated at its middle position. The masses of the trunk, arms, and head are lumped at the hip link. This model moves forward under the action of gravity, between configurations A and C, until foot strike. (V_{xf}, V_{yf}, V_{zf}) denotes the desired velocity of the hip link at lift-off and $(\dot{X}_{C,td}, \dot{Y}_{C,td}, \dot{Z}_{C,td})$ denotes the actual velocity of the hip link at touch-down. The plot (**b**) shows the configuration of the hip link and two legs when the robot system moves into the positive Y-axis direction. Note that when the robot switches from a support phase to a flight phase, its total mass m_g is divided into three parts, i.e., M, M_1, and M_2, which are used to control the rate of rotation of the robot's center of mass

$$
\begin{aligned}
&+ M_2\dot{Z}_{2j}/2 - m_g g T_f(r-1)/2 \\
&i = 1,2 \text{ (left or right foot)},\ j = A\ (r=1),\ B\ (r=2), \\
&C\ (r=3) \text{ (breakpoints)}
\end{aligned} \tag{18}
$$

where $m_g = M + M_1 + M_2$ and T_f denotes the duration of the flight phase.

The center of mass of the approximated running model $(\overline{X}_j,\ \overline{Y}_j,\ \overline{Z}_j)$ follows a ballistic curve when the robot flies through the air. The parabolic curve is described by (18). Thus,

$$
\dot{\overline{X}}_j = \dot{\overline{X}}_{lo}, \qquad \dot{\overline{Y}}_j = \dot{\overline{Y}}_{lo}, \qquad \dot{\overline{Z}}_j = \dot{\overline{Z}}_{lo} - g T_f(r-1)/2 \tag{19}
$$

where $\dot{\overline{X}}_{lo}$, $\dot{\overline{Y}}_{lo}$, and $\dot{\overline{Z}}_{lo}$ denote the initial velocities of the model's center of mass.

Similarly, the hip describes a parabola after lift-off, since the model's center of mass exists very close to it. Thus,

$$
\begin{aligned}
\dot{X}_j &= \dot{X}_A(1.0 + 2.0\sigma(r-1) - \sigma(r-1)^2), \\
\dot{Y}_j &= \dot{Y}_A(1.0 + 2.0\sigma(r-1) - \sigma(r-1)^2), \\
\dot{Z}_j &= \dot{Z}_A - g T_f(r-1)/2
\end{aligned} \tag{20}
$$

where $\dot{X}_A$, $\dot{Y}_A$, and $\dot{Z}_A$ denote the initial velocities of the hip link at lift-off which are determined by the desired position and velocity of the hip link at the end of the support phase, as given in Sect. 4.2. Even though the velocity of the center of mass in the X-axis and Y-axis directions switches to a constant value after lift-off, the velocity of the hip follows a parabolic curve after lift-off in such a way as to cause the acceleration of the hip link at lift-off to be continuous. σ denotes a positive constant value which is manually tuned. It is assumed that the inertia of each link in the running model is neglected. The modified components $((\vec{H}'_G)_x, (\vec{H}'_G)_y, (\vec{H}'_G)_z)$ of the angular momentum in (4) are described by the following equations:

$$
\begin{aligned}
(\vec{H}'_G)_x &= M_1/4\{(Y_{1j}-\overline{Y}_j)(\dot{Z}_{1j}-\dot{\overline{Z}}_j)\\
&\quad -(Z_{1j}-\overline{Z}_j)(\dot{Y}_{1j}-\dot{\overline{Y}}_j)\}\\
&\quad +M_2/4\{(Y_{2j}-\overline{Y}_j)(\dot{Z}_{2j}-\dot{\overline{Z}}_j)\\
&\quad -(Z_{2j}-\overline{Z}_j)(\dot{Y}_{2j}-\dot{\overline{Y}}_j)\}\\
&\quad +M\{(Y_j-\overline{Y}_j)(\dot{Z}_j-\dot{\overline{Z}}_j)\\
&\quad -(Z_j-\overline{Z}_j)(\dot{Y}_j-\dot{\overline{Y}}_j)\},\\
(\vec{H}'_G)_y &= M_1/4\{(Z_{1j}-\overline{Z}_j)(\dot{X}_{1j}-\dot{\overline{X}}_j)\\
&\quad -(X_{1j}-\overline{X}_j)(\dot{Z}_{1j}-\dot{\overline{Z}}_j)\}\\
&\quad +M_2/4\{(Z_{2j}-\overline{Z}_j)(\dot{X}_{2j}-\dot{\overline{X}}_j)\\
&\quad -(X_{2j}-\overline{X}_j)(\dot{Z}_{2j}-\dot{\overline{Z}}_j)\}\\
&\quad +M\{(Z_j-\overline{Z}_j)(\dot{X}_j-\dot{\overline{X}}_j)\\
&\quad -(X_j-\overline{X}_j)(\dot{Z}_j-\dot{\overline{Z}}_j)\},\\
(\vec{H}'_G)_z &= M_1/4\{(X_{1j}-\overline{X}_j)(\dot{Y}_{1j}-\dot{\overline{Y}}_j)\\
&\quad -(Y_{1j}-\overline{Y}_j)(\dot{X}_{1j}-\dot{\overline{X}}_j)\}\\
&\quad +M_2/4\{(X_{2j}-\overline{X}_j)(\dot{Y}_{2j}-\dot{\overline{Y}}_j)\\
&\quad -(Y_{2j}-\overline{Y}_j)(\dot{X}_{2j}-\dot{\overline{X}}_j)\}\\
&\quad +M\{(X_j-\overline{X}_j)(\dot{Y}_j-\dot{\overline{Y}}_j)\\
&\quad -(Y_j-\overline{Y}_j)(\dot{X}_j-\dot{\overline{X}}_j)\}
\end{aligned}
\tag{21}
$$

where the modified angular momenta, $((\vec{H}'_G)_x$, $(\vec{H}'_G)_y$, $(\vec{H}'_G)_z)$, are set to proper values in order to obtain the position and velocity of two legs at each configuration. Their allowable ranges are determined by the support phase trajectories of the hip link and two legs, as given in Sect. 3. The configurations and speeds of two feet at each breakpoint can be obtained by (18) and (21), when the hip link follows the flight phase trajectory given in (20), as shown in parts (a) and (b) of Fig. 3. The total number of unknown variables with respect to the breakpoints is equal to the number of equations in (18) and (21), which represents 18 equations. Quintic interpolating polynomials are used to specify the position, velocity, and acceleration at the beginning and end of path segments which connect the speeds and configurations of two feet at each breakpoint.

4.2 Support phase trajectories

A spring-like leg motion which operates a supporting leg like a linear spring within proper conditions is generally achieved based on the spring-loaded inverted pendulum model, as shown in Fig. 4. The SLIP model yields symmetric trajectories under the assumption that the robot model is composed of a body of mass m_g and a massless supporting leg with a linear spring of stiffness k_{leg}, and the ZMP exists in the center of the supporting foot, as given in Appendix C. When a SLIP moves symmetrically, its energy is stored in the leg spring, in the motion of the body mass, and in the position of the body mass (Raibert 1986). The total energy E_{total} at any time in the sagittal plane should thus be given by

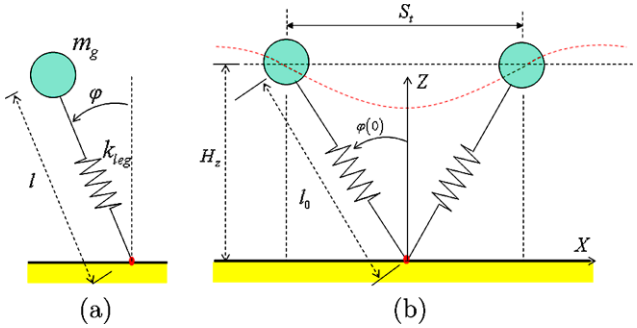

Fig. 4 Spring Loaded Inverted Pendulum Model (SLIP model) with a body of point mass m_g and a massless leg spring for running in the sagittal plane. (**a**) The leg spring is characterized by the stiffness k_{leg} and the nominal length l_0 which is the leg length at touch-down and lift-off, and forms an angle φ with the vertical axis, while its length at any time is l. (**b**) The model moves with symmetry at touch-down and lift-off during the support phase, and the leg neither rebounds nor slides after touch-down

$$E_{total} = 1/2m_g(\dot{X}^2+\dot{Z}^2)+m_g gZ+1/2k_{leg}(l_0-l)^2. \tag{22}$$

Inserting $X = l\sin\varphi$ and $Z = l\cos\varphi$ into (22) leads to

$$
\begin{aligned}
2E_{total} &= m_g(\dot{l}^2+2gl\cos\varphi+l^2\dot{\varphi}^2)+k_{leg}(l_0-l)^2\\
&= m_g(\dot{l}^2+2gl\cos\varphi+l^2\dot{\varphi}^2)\\
&\quad +k_{leg}(\sqrt{{H_z}^2+(S_t/2)^2}-l)^2
\end{aligned}
\tag{23}
$$

where l_0 is equal to $\sqrt{{H_z}^2+(S_t/2)^2}$ at touch-down and lift-off. Equation (23) states that the total energy requires a proper adjustment of locomotion parameters such as the duration of a support phase T_s, the stiffness of the supporting leg k_{leg}, the stride of a support phase S_t, and the height of the hip link H_z at touch-down and lift-off, depending on the robot model. Figure 5 shows the total energy curves during the support phase when the SLIP model follows the symmetric trajectory given in Appendix C. The least amount of the total energy varies according to variations of locomotion parameters. As the vertical height of the hip link H_z at touch-down and lift-off gets higher, the total energy increases proportionally. Similarly, the longer the stride of the support phase S_t is, the larger the total energy gets. It is important to note that the vertical height of the hip link Z

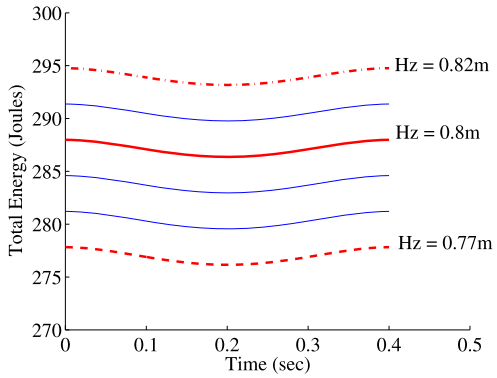

(a)Total Energy (E_{total}) vs. Height (H_z)

$S_t = 0.3\ [m]$, $k_{leg} = 8500.0\ [N/m]$, $T_s = 0.4\ [s]$

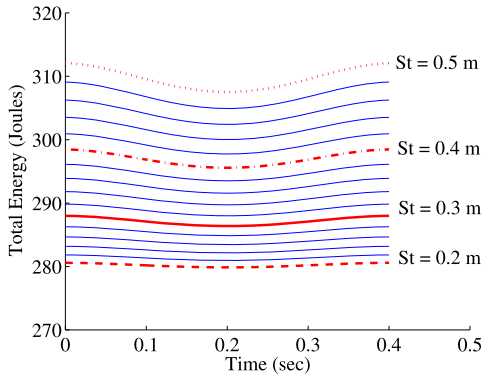

(b)Total Energy (E_{total}) vs. Stride (S_t)

$T_s = 0.4\ [s]$, $k_{leg} = 8500.0\ [N/m]$, $H_z = 0.8\ [m]$

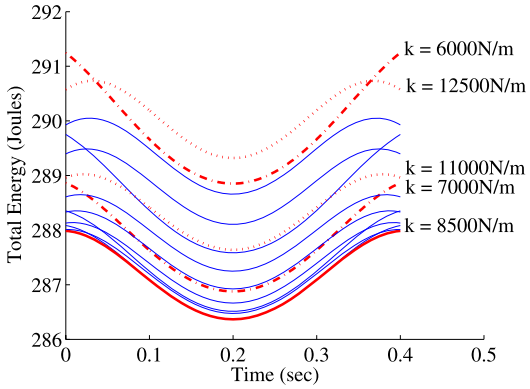

(c)Total Energy (E_{total}) vs. Stiffness (k_{leg})

$S_t = 0.3\ [m]$, $T_s = 0.4\ [s]$, $H_z = 0.8\ [m]$

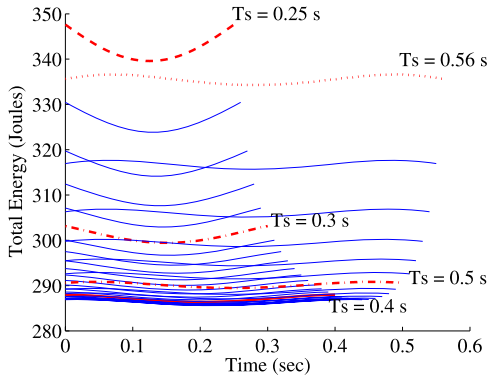

(d)Total Energy (E_{total}) vs. Time (T_s)

$S_t = 0.3\ [m]$, $k_{leg} = 8500.0\ [N/m]$, $H_z = 0.8\ [m]$

Fig. 5 Total energy of the SLIP model during the support phase according to variations of locomotion parameters (four variables): the duration of a support phase T_s, the stiffness of the supporting leg k_{leg}, the stride of a support phase S_t, and the vertical height of the hip link H_z at touch-down and lift-off. In each diagram (**a**–**d**), three variables are kept constant. All the energy curves are not kept constant during the support phase when the body of the SLIP model follows the symmetric trajectory which is derived from the linearized mathematical model under an assumption that the angle formed between the vertical axis and the leg spring varies within a narrow range. If the angle varies within a wide range, the linearized model needs to add additional energy to the system by delivering torques through joint actuators. However, these do not distort the arguing point of this paper. For example, the vertical height of the hip link of the robot with the total mass $m_g =$ 35.0 [kg] used in the simulations is 0.9 [m] when its knee is stretched fully. When $H_{z,min} = 0.73$ [m], $H_{z,max} = 0.82$ [m], $S_{t,min} = 0.2$ [m], $S_{t,max} = 0.35$ [m], the locomotion parameters for the SLIP-like motion are selected as $T_s = 0.4$ [s], $S_t = 0.3$ [m], $k_{leg} = 8500.0$ [N/m], and $H_z = 0.8$ [m]

between the start and the end of the support phase as well as the vertical height of the hip link H_z at touch-down and lift-off should be determined within the allowable range to prevent a segmented leg of a biped robot from being fully stretched or being fully folded so that a singular configuration ($\det(J_l) = 0$ or $\det(J_r) = 0$) and the collision between links do not occur in any case, i.g., $H_{z,min} < H_z$ or $Z < H_{z,max}$. In addition, the stride of the support phase S_t should be determined within the allowable range to avoid a singular configuration according to the desired forward velocity of the robot and the chosen foothold compatible with the environment, i.g., $S_{t,min} < S_t < S_{t,max}$. The desired velocity of the robot is determined by (67). Thus,

$$V_{xf} = -\frac{\sqrt{g/H_z}S_t(1+e^{T_s\sqrt{g/H_z}})}{2(1-e^{T_s\sqrt{g/H_z}})} \tag{24}$$

where the desired velocity of the robot V_{xf} depends more on the stride of the robot during a support phase S_t and the duration of a support phase T_s than the vertical height of the hip link H_z at touch-down and lift-off. Plots (c) and

(d) of Fig. 5 show the curves of the total energy according to variations of the stiffness of the supporting leg k_{leg} and the duration of a support phase T_s. It is obvious that the smaller the stiffness of the supporting leg k_{leg} is, the lower the vertical height of the hip link in the middle of the support phase gets and the more frequently the collision between links joined to knee joints of the biped robot occurs. Therefore, the locomotion parameters are determined in this order: $H_z \rightarrow S_t \rightarrow k_{leg} \rightarrow T_s$. The chosen locomotion parameters are not global optimum solutions but local optimum solutions, since they are constrained by the kinematic structure and locomotion conditions of the biped robot. Thus, the locomotion parameters leads to a locally optimized trajectory so that controlling the biped robot close to it reduces energy consumption. The least amount of the energy consumption varies according to the robot model and the targeted forward velocity.

In addition to the symmetric SLIP-like motion which are determined by the locomotion parameters, bipedal running requires asymmetric behavior. The asymmetric trajectory is generated from the SLIP model and the approximated running model, as shown in Fig. 3. The vertical motion of the hip link along the Z-axis forces the robot to absorb the large vertical force caused by an impulsive collision at every footfall and to store the elastic energy in the supporting leg immediately following its impact with the ground, to be released later as the robot rebounds into the air. The vertical movement along the Z-axis is specified with the SLIP model in the vertical direction. The response curve of the mass-spring system, in which the mass (hip link) is subjected to its initial configuration and speed at touch-down, reaches a maximum compression value in the middle of the support phase. When the leg spring is shortened to its minimum length, energy stored in the leg spring is equal to the sum of potential energy in the vertical position of the body mass and kinetic energy in the vertical velocity of the body mass. Thus,

$$1/2k_{leg}\xi^2 = 1/2m_g\dot{Z}_{C,td}^2 + m_g g\xi. \tag{25}$$

The maximum depth ξ when the spring is compressed can be found with (25).

$$\xi = (m_g g + \sqrt{m_g^2 g^2 + k_{leg} m_g \dot{Z}_{C,td}^2})/k_{leg} \tag{26}$$

where $Z_{C,td}$ and $\dot{Z}_{C,td}$ denote the initial vertical position and velocity of the hip link at touch-down, respectively. Immediately on detecting a foot contact with the ground, the compression depth ξ is determined depending on the actual initial vertical velocity of the hip link. Therefore, the Z-axis trajectory is constrained by the actual position and velocity of the hip link at touch-down, the movement distance of the hip link ξ at half duration of the support phase, and the desired position and velocity of the hip link at take-off. When the configuration and speed of the hip link at touch-down and lift-off in the Z-axis direction are chosen as $[Z_{C,td},\ \dot{Z}_{C,td}]$ and $[Z_A,\ \dot{Z}_A]$, respectively, a fourth interpolating polynomial is chosen to satisfy these constraints.

$$\begin{aligned}
Z(t) &= a_0 + a_1 t + a_2 t^2 + a_3 t^3 + a_4 t^4,\\
a_0 &= Z_{C,td}, a_1 = \dot{Z}_{C,td},\\
a_2 &= (11Z_A - 16\xi - 4T_s\dot{Z}_{C,td} + T_s\dot{Z}_A)\\
&\quad - 11Z_{C,td})/T_s^2,\\
a_3 &= (-18Z_A + 32\xi + 5T_s\dot{Z}_{C,td} - 3T_s\dot{Z}_A)\\
&\quad + 18Z_{C,td})/T_s^3,\\
a_4 &= 2.0(4Z_A - 8\xi - T_s\dot{Z}_{C,td} + T_s\dot{Z}_A) - 4Z_{C,td})/T_s^4
\end{aligned} \tag{27}$$

where $\dot{Z}_A$ $(= V_{zf})$ and Z_A $(= H_z)$ are the desired vertical velocity and position of the hip link at lift-off, respectively. Note that the vertical accelerations of the hip link at touch-down and lift-off are the same as $-g$ and then are omitted from the interpolating polynomial.

The configuration, speed, and acceleration of the hip link at touch-down and lift-off in the X-axis direction are chosen as $[X_{C,td},\ \dot{X}_{C,td},\ \ddot{X}_{C,td}]$ and $[X_A,\ \dot{X}_A,\ \ddot{X}_A]$, respectively. The speed of the hip link at lift-off, $\dot{X}_A$, is determined by (67), which is related to the desired position of the hip link at lift-off, X_A, and the stride of the robot, S_t. Thus,

$$\dot{X}_A = \frac{1 + e^{\omega_1 T_s}}{1 - e^{\omega_1 T_s}} \omega X_A \tag{28}$$

where $\omega_1 = \sqrt{g/Z_A} = \sqrt{g/H_z}$. The configuration and speed of the hip link in the middle of the support phase $[X_{CA},\ \dot{X}_{CA}]$ are identical to those of the hip link in the middle of the support phase of the SLIP model. Thus,

$$\begin{aligned}
X_{CA} &= \frac{1}{2}\left(X_A + \frac{1}{\omega_1}\dot{X}_A\right) e^{\omega_1 T_s/2}\\
&\quad + \frac{1}{2}\left(X_A - \frac{1}{\omega_1}\dot{X}_A\right) e^{-\omega_1 T_s/2},\\
\dot{X}_{CA} &= \frac{1}{2}\left(X_A + \frac{1}{\omega_1}\dot{X}_A\right) \omega_1 e^{\omega_1 T_s/2}\\
&\quad - \frac{1}{2}\left(X_A - \frac{1}{\omega_1}\dot{X}_A\right) \omega_1 e^{-\omega_1 T_s/2}.
\end{aligned} \tag{29}$$

Therefore, the support phase trajectory of the hip link in the X-axis direction would be completely determined using a seventh-order interpolating polynomial as a function of time t. $\ddot{X}_{C,td}$ and $\ddot{X}_A$ are set at zero, since no distinct advantage results from different chosen values. Similarly,

the configuration, speed, and acceleration of the hip link at touch-down and lift-off in the Y-axis direction are chosen as $[Y_{C,td},\ \dot{Y}_{C,td},\ \ddot{Y}_{C,td}]$ and $[Y_A,\ \dot{Y}_A,\ \ddot{Y}_A]$, respectively. The speed of the hip link at lift-off, $\dot{Y}_A$, is determined based on the desired position of the hip link at lift-off, Y_A. Thus,

$$\dot{Y}_A = \frac{1 - e^{\omega_1 T_s}}{1 + e^{\omega_1 T_s}} \omega_1 Y_A. \tag{30}$$

The support phase trajectory of the hip link in the Y-axis direction would be completely determined using a fifth-order interpolating polynomial as a function of time t:

$$\begin{aligned}
Y(t) &= a_0 + a_1 t + a_2 t^2 + a_3 t^3 + a_4 t^4 + a_5 t^5, \\
a_0 &= Y_{C,td},\ a_1 = \dot{Y}_{C,td},\ a_2 = \ddot{Y}_{C,td}/2.0, \\
a_3 &= (20.0Y_A - 20.0Y_{C,td} - (8.0\dot{Y}_A + 12.0\dot{Y}_{C,td})T_s \\
&\quad - T_s^2(3.0\ddot{Y}_{C,td} - \ddot{Y}_A))/2.0T_s^3, \\
a_4 &= (30.0Y_{C,td} - 30.0Y_A + (14.0\dot{Y}_A + 16.0\dot{Y}_{C,td})T_s \\
&\quad + T_s^2(3.0\ddot{Y}_{C,td} - 2.0\ddot{Y}_A))/2.0T_s^4, \\
a_5 &= (12.0Y_A - 12.0Y_{C,td} - 6.0\dot{Y}_A + 6.0\dot{Y}_{C,td})T_s \\
&\quad - T_s^2(\ddot{Y}_{C,td} - \ddot{Y}_A))/2.0T_s^5
\end{aligned} \tag{31}$$

where $\ddot{Y}_{C,td} = 0.0$, $\ddot{Y}_A = 0.0$.

The configurations and speeds of a freely swing foot at the beginning and end of the support phase become identical to those of a rear foot (left foot) at the end of the flight phase and a front foot (right foot) at the beginning of the flight phase, respectively, as given in Sect. 4.1. Quintic interpolating polynomials for a swing foot $[X_{sf},\ Y_{sf},\ Z_{sf}]$ are chosen to satisfy these conditions. When the configuration, speed, and acceleration of the swing foot at touch-down and lift-off are chosen as $[Z_{1C,td},\ \dot{Z}_{1C,td},\ \ddot{Z}_{1C,td}]$ and $[Z_{2A},\ \dot{Z}_{2A},\ \ddot{Z}_{2A}]$, respectively, the tracking function for Z_{sf} during the support phase would be as a function of time t:

$$\begin{aligned}
Z_{sf}(t) &= a_0 + a_1 t + a_2 t^2 + a_3 t^3 + a_4 t^4 + a_5 t^5, \\
a_0 &= Z_{1C,td},\ a_1 = \dot{Z}_{1C,td},\ a_2 = 1/2\ddot{Z}_{1C,td}, \\
a_3 &= (20Z_{2A} - 20Z_{1C,td} - (8\dot{Z}_{2A} + 12\dot{Z}_{1C,td})T_s \\
&\quad - (3\ddot{Z}_{1C,td} - \ddot{Z}_{2A})T_s^2)/2T_s^3, \\
a_4 &= (30Z_{2A} - 30Z_{1C,td} + (14\dot{Z}_{2A} + 16\dot{Z}_{1C,td})T_s \\
&\quad + (3\ddot{Z}_{1C,td} - 2\ddot{Z}_{2A})T_s^2)/2T_s^4, \\
a_5 &= (12Z_{2A} - 12Z_{1C,td} - (6\dot{Z}_{2A} + 6\dot{Z}_{1C,td})T_s \\
&\quad - (\ddot{Z}_{1C,td} - \ddot{Z}_{2A})T_s^2)/2T_s^5
\end{aligned} \tag{32}$$

where $\ddot{Z}_{2A} = -g$, and $\ddot{Z}_{1C,td} = 0.0$. The polynomial function for $X_{sf}(t)$ can be found as a function of time t in the same manner. The backward velocity of a front foot (right foot) at the end of the flight phase with respect to the hip is determined to be matched to the backward velocity of the ground. Thus, $\dot{X}_{2C,td} \approx 0.0$. In addition, $Y_{sf}(t)$ is kept constant during the support phase if the control system does not change direction.

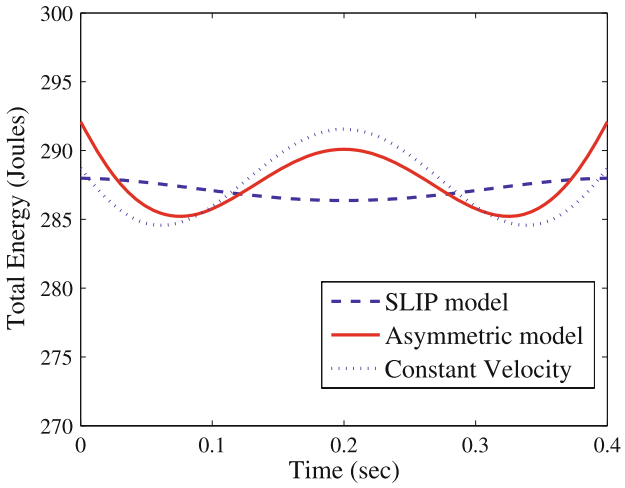

Fig. 6 Total energy comparison among three models: SLIP model, asymmetric model, and model in which the velocity of the hip link in the X-axis direction is kept constant and moves like a bouncing elastic ball in the vertical direction (a kind of asymmetric model). $T_s = 0.4$ [s], $S_t = 0.3$ [m], $k_{leg} = 8500$ [N/m], and $H_z = 0.8$ [m] are used

In brief, the asymmetric trajectory can be modified online according to the initial states of the biped robot at touch-down and lift-off, and the desired running speed. By comparison with the total energy at any time during a support phase, the asymmetric trajectory has almost the same energy curve as the other models, as shown in Fig. 6(a). The model in which the horizontal velocity of the hip link in the X-axis direction is kept constant and varies according to the velocity of the robot at touch-down is a kind of asymmetric model, but is not suitable to purposely transit gaits and change the desired horizontal velocity.

4.3 Nonslip condition

A running biped robot may slip on smooth surfaces or relatively high friction surfaces since its foot is moving fast with respect to the ground at touch-down and lift off. In general, the robot control system can not detect and avoid or prepare for this dangerous situation, and the robot will almost always immediately fall to the ground. This paper does not put its focus on any strategy to overcome foot slipping of biped robots on a suddenly encountered slippery surface (Boone and Hodgins 1997; Kwon and Park 2002). Rather, it pays an attention to a highly effective asymmetric trajectory in order to prevent or minimize foot slips and maintain steady-state running.

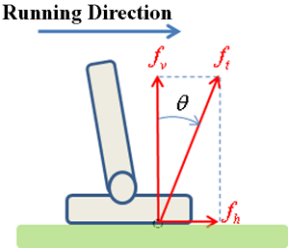

Fig. 7 When a foot is in contact with the ground in the sagittal plane, it creates a force f_t with tangential component f_h and normal component f_v on the ground

Slipping occurs when the tangential component $f_h \in \Re^1$ of the external force exerted on the foot exceeds the maximum force of the static friction force, which is proportional to the normal component $f_v \in \Re^1$ of the external force. Under this interaction, Coulomb's law states that slipping begins when $|f_h| > \mu_s |f_v|$, and slipping occurs when $|f_h| = \mu_d |f_v|$. μ_s and μ_d denotes the static coefficient and dynamic coefficient of friction that are a function of the materials which are in contact. This implies that the range of the tangential force which can be applied at a contact is given by

$$|f_h| \leq \mu_s |f_v| \tag{33}$$

where $|*|$ denotes the absolute value of scalar $*$. Interpreting (33) geometrically leads to

$$\theta = \tan^{-1} |f_h|/|f_v| < \tan^{-1} \mu_s |f_v|/|f_v| = \tan^{-1} \mu_s \tag{34}$$

where θ is the angle between the foot's force f_t and the normal force f_v and should be limited so that the supporting foot should not slip at a contact between its sole and the ground. Therefore, the running trajectory must be satisfied with (34). In the sagittal plane,

$$\theta = \tan^{-1} \frac{|m_g \ddot{X}_g|}{|m_g(\ddot{Z}_g + g)|} < \tan^{-1} \mu_s \tag{35}$$

where $f_h = F_x = m_g \ddot{X}_g$ and $f_v = F_z = m_g(\ddot{Z}_g + g)$ in (55) under the assumption that no external force exists except at the soles, as shown in Fig. 7. Equation (35) states that the larger the magnitude of $\ddot{Z}_g$ gets and the smaller the magnitude of $\ddot{X}_g$ becomes, the lower the risk for slipping gets, and also $|\ddot{X}_g| < \mu_s |\ddot{Z}_g + g|$. It is important that the normal component f_v of the external force after touch-down is sufficiently large so that a foot does not slip at a contact between its sole and the ground. Hence, the downward vertical acceleration of the front foot at the end of the flight phase $\ddot{Z}_{2C,td}$ is selected to be 1.5 times larger than the gravity acceleration, if $|\ddot{Z}_g| \geq g$. On the other hand, the horizontal acceleration of the foot at touch-down $\ddot{X}_{2C,td}$ based on $|\ddot{X}_g| < \mu_s |\ddot{Z}_g + g|$ is chosen to be zero.

5 Impedance controller for running

For stable running, the supporting foot in the support phase must not move on the ground whereas both freely swinging feet in the flight phase should be in the air and must not strike the ground. And the supporting (front) leg must reduce large impact forces generated at the moment of contacting with the ground and does not bounce back from the ground. This situation means that a controller for running of biped robots should be able to manage elegantly the large external forces and track the desired trajectories. Considering these characteristics, an impedance controller is designed and applied according to each phase.

The supporting leg of the support phase must support the total weight of the biped robot and push ahead the hip and upper body. This part is controlled based on the desired impedance model of the hip link specified with respect to the supporting foot on the ground. Also, the freely swinging leg and upper body must move relatively from the hind to the front of the hip link in the forward direction. These two parts are controlled based on the desired impedance models of the swing foot and upper body specified with respect to the hip link under the assumption that the hip link follows its predetermined trajectory according to its desired impedance characteristics as shown in part (a) of Fig. 8. In the flight phase, two feet are in the air. The two swing feet are compressed into following the desired trajectory on the basis of the hip link. Thus, the impedance models of the two feet and upper body which are to be controlled are defined from the hip link as shown in part (b) of Fig. 8.

For notational convenience, in the following sections the impedance control laws for the legs will be driven under the assumption that the right leg is supporting and the left leg is swinging in the support phase. In addition, the left leg is in front of the right leg in the flight phase. It is assumed that each foot is equipped with force sensors and the body contains a acceleration sensor, three Gyro sensors and absolute position sensors.

5.1 Impedance control for the support phase

The impedance control of the swing left leg is obtained from the relationship between the joint velocity $\dot{\vec{q}}_l \in \Re^6$ of the left leg and the velocity vector $\dot{\vec{x}}_{lf} \in \Re^6$ of the left foot represented by the absolute coordinates in Fig. 1.

$$\ddot{\vec{x}}_{lf} = \ddot{\vec{x}}_h + R_0 \ddot{\vec{x}}^h_{lf} + \dot{\vec{\Omega}}_l \tag{36}$$

where

$$\dot{\vec{x}}_{lf} = \begin{bmatrix} \dot{\vec{x}}^0_{lf} \\ \vec{\omega}^0_{lf} \end{bmatrix}, \qquad \dot{\vec{x}}_h = \begin{bmatrix} \dot{\vec{x}}^0_h \\ \vec{\omega}^0_h \end{bmatrix},$$

$$\dot{\vec{x}}^h_{lf} = \begin{bmatrix} \dot{\vec{x}}^h_{lf} \\ \vec{\omega}^h_{lf} \end{bmatrix} = J_l \dot{\vec{q}}_l, \qquad \ddot{\vec{x}}^h_{lf} = J_l \ddot{\vec{q}}_l + \dot{J}_l \dot{\vec{q}}_l,$$

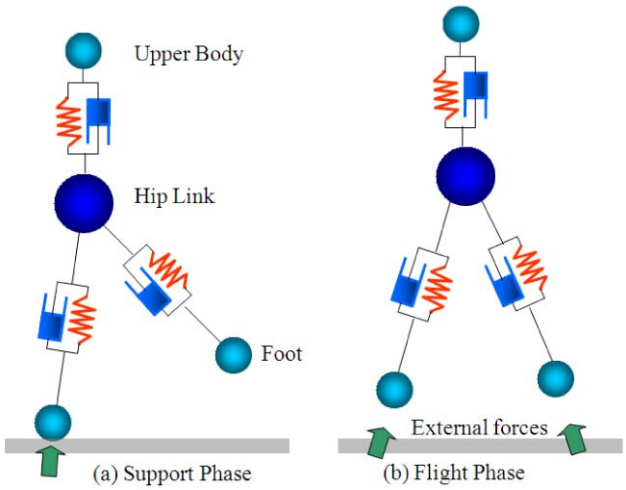

Fig. 8 Four limbs and body of a biped robot in the flight and support phases are modeled as mechanical impedances with corresponding stiffness, mass and damping terms. The mechanical impedance is adjusted to follow the predetermined trajectory and control the contact force between the foot and the environment

$$\vec{\Omega}_l = \begin{bmatrix} 2\vec{\omega}_h^0 \times R_h^0 \dot{\vec{x}}_{lf}^h + \dot{\vec{\omega}}_h^0 \times R_h^0 \vec{x}_{lf}^h + \vec{\omega}_h^0 \times (\vec{\omega}_h^0 \times R_h^0 \vec{x}_{lf}^h) \\ \vec{\omega}_h^0 \times R_h^0 \vec{\omega}_{lf}^h \end{bmatrix},$$

$$R_0 = \begin{bmatrix} R_h^0 & 0_{3\times 3} \\ 0_{3\times 3} & R_h^0 \end{bmatrix},$$

and $R_h^0 \in \Re^{3\times 3}$ is the orientation matrix of the body center coordinates represented by the absolute coordinates. Vectors $\dot{\vec{x}}_{lf}^0 \in \Re^3$ and $\vec{\omega}_{lf}^0 \in \Re^3$ indicate the linear velocity and angular velocity of the left foot, respectively. Assuming that we are away from workspace singularities or singular configurations so that the determinant of the Jacobian matrix is not equal to zero, the inverse acceleration transformation equation is derived from (36).

$$\ddot{\vec{q}}_l = (R_0 J_l)^{-1}(\ddot{\vec{x}}_{lf} - \ddot{\vec{x}}_h - R_0 \dot{J}_l \dot{\vec{q}}_l - \vec{\Omega}_l) \tag{37}$$

where $J_l \in \Re^{6\times 6}$ and $\dot{\vec{x}}_{lf}^h \in \Re^6$ are the Jacobian matrix and velocity vector of the left foot with respect to body center coordinates, respectively. Suppose that the desired impedance model of the swing left leg is defined as the following equation:

$$\begin{aligned} &M_L \ddot{\tilde{x}}_{lf} + D_L \dot{\tilde{x}}_{lf} + E_L \tilde{x}_{lf} = \vec{0} \quad \text{or} \\ &\ddot{\tilde{x}}_{lf} = \ddot{\vec{x}}_{lf,d} - M_L^{-1}(D_L \dot{\tilde{x}}_{lf} + E_L \tilde{x}_{lf}) \end{aligned} \tag{38}$$

where $\dot{\tilde{x}}_{lf} = \dot{\vec{x}}_{lf} - \dot{\vec{x}}_{lf,d}$ and superscript 'd' denotes the desired value. The desired mass, damping, and stiffness matrices (M_L, D_L and E_L) are assumed to be constant and positive definite. Substituting (37) and (38) into the torque equation related to the left leg in (1), the torque vector of the left leg is obtained to follow asymptotically the desired impedance characteristics.

$$\begin{aligned} \vec{\tau}_l = H_l (R_0 J_l)^{-1} &(\ddot{\vec{x}}_{lf,d} - M_L^{-1}(D_L \dot{\tilde{x}}_{lf} + E_L \tilde{x}_{lf}) \\ &- \ddot{\vec{x}}_h - R_0 \dot{J}_l \dot{\vec{q}}_l - \vec{\Omega}_l) + D_l \vec{f}_l + K_l \ddot{\vec{x}}_h + L_l. \end{aligned} \tag{39}$$

Next, the joint torque of the right leg is computed using the predefined impedance model of the hip link and (1). The torque equations related to the left leg and upper body in (1) are transformed into the following equations:

$$\begin{aligned} \ddot{\vec{q}}_l &= H_l^{-1}(\vec{\tau}_l - K_l \ddot{\vec{x}}_h - D_l \vec{f}_l - L_l), \\ \ddot{\vec{q}}_b &= H_b^{-1}(\vec{\tau}_b - K_b \ddot{\vec{x}}_h - L_b). \end{aligned} \tag{40}$$

The linear and angular accelerations of the supporting foot must be equal to zero so that the foot is fixed on the ground, regardless of the external forces at its landing on the ground. A constraint equation with zero linear and angular accelerations of the supporting foot is derived from (36).

$$A_r \ddot{\vec{q}}_r + B_r \ddot{\vec{x}}_h + C_r = \vec{0} \quad \text{or} \quad \ddot{\vec{q}}_r = -A_r^{-1}(C_r + B_r \ddot{\vec{x}}_h) \tag{41}$$

where A_r, B_r and C_r are the coefficient matrices. Inserting (40) and (41) into the lower part equation of (1) leads to

$$\tilde{R} \ddot{\vec{x}}_h + \tilde{S} + P_r \vec{f}_r = \vec{0} \tag{42}$$

where

$$\begin{aligned} \tilde{R} &= R - Q_r A_r^{-1} B_r - Q_l H_l^{-1} K_l - Q_b H_b^{-1} K_b, \\ \tilde{S} &= S + Q_l H_l^{-1}(\vec{\tau}_l - D_l \vec{f}_l - L_l) + Q_b H_b^{-1}(\vec{\tau}_b - L_b) \\ &\quad - Q_R A_r^{-1} C_r. \end{aligned}$$

Suppose the desired impedance of the hip link at its center is

$$\begin{aligned} &M_h \ddot{\tilde{x}}_h + D_h \dot{\tilde{x}}_h + E_h \tilde{x}_h = \vec{0} \quad \text{or} \\ &\ddot{x}_h = \ddot{x}_{h,d} - M_h^{-1}(D_h \dot{\tilde{x}}_h + E_h \tilde{x}_h) \end{aligned} \tag{43}$$

where $\dot{\tilde{x}}_h = \dot{\vec{x}}_h - \dot{\vec{x}}_{h,d}$. The desired mass, damping, and stiffness matrices about the hip link (M_h, D_h and E_h) are assumed to be constant and positive definite. This equation implies that the hip follows asymptotically the desired trajectory. Substituting (42) and (43) into the torque equation related to the right leg in (1), the joint torque of the supporting right leg results in

$$\begin{aligned} \vec{\tau}_r = (K_r - H_r A_r^{-1} B_r - D_r P_r^{-1} \tilde{R})(\ddot{x}_{h,d} - M_h^{-1}(D_h \dot{\tilde{x}}_h \\ + E_h \tilde{x}_h)) + L_r - H_r A_r^{-1} C_r - D_r P_r^{-1} \tilde{S}. \end{aligned} \tag{44}$$

5.2 Impedance control for the flight phase

The joint torque for the rear right leg in order for the biped robot to take off on the ground is computed using the impedance model predefined from the hip link and (1). The torque equations related to the right leg and upper body in (1) are transformed into the following equations:

$$\begin{aligned}\ddot{\vec{q}}_l &= H_l^{-1}(\vec{\tau}_l - K_l\ddot{\vec{x}}_h - D_l\vec{f}_l - L_l),\\ \ddot{\vec{q}}_b &= H_b^{-1}(\vec{\tau}_b - K_b\ddot{\vec{x}}_h - L_b).\end{aligned} \tag{45}$$

Substituting (45) into the lower part equation of (1) leads to

$$\tilde{R}\ddot{\vec{x}}_h + \tilde{S} + Q_r\ddot{\vec{q}}_r = \vec{0} \tag{46}$$

where

$$\begin{aligned}\tilde{R} &= R - Q_l H_l^{-1}K_l - Q_b H_b^{-1}K_b,\\ \tilde{S} &= S + Q_l H_l^{-1}(\vec{\tau}_l - L_l) + Q_b H_b^{-1}(\vec{\tau}_b - L_b)\\ &\quad + (P_l - Q_l H_l^{-1}D_l)\vec{f}_l + P_r\vec{f}_r.\end{aligned}$$

Suppose the desired impedance of the rear right leg is

$$\begin{aligned}&M_R\ddot{\tilde{x}}_{rf} + D_R\dot{\tilde{x}}_{rf} + E_R\tilde{x}_{rf} = -\vec{f}_r \quad \text{or}\\ &\ddot{x}_{rf} = \ddot{x}_{rf,d} + M_R^{-1}(-\vec{f}_r - D_R\dot{\tilde{x}}_{rf} - E_R\tilde{x}_{rf})\end{aligned} \tag{47}$$

where $\dot{\tilde{x}}_{rf} = \dot{\vec{x}}_{rf} - \dot{\vec{x}}_{rf,d}$. M_R, D_R and E_R denote the desired mass, damping ratio and stiffness about the rear right leg, respectively. This equation implies that the swing right leg follows asymptotically the desired trajectory. Similarly, the inverse acceleration transformation is obtained from the relationship between the joint velocity $\dot{\vec{q}}_r \in \Re^6$ of the right leg and the Cartesian velocity vector $\dot{\vec{x}}_{rf} \in \Re^6$ of the right foot about O in Fig. 1. Thus,

$$\ddot{\vec{q}}_r = (R_0 J_r)^{-1}(\ddot{\vec{x}}_{rf} - \ddot{\vec{x}}_h - R_0\dot{J}_r\dot{\vec{x}}_{rf} - \vec{\Omega}_r) \tag{48}$$

where $J_r \in \Re^{6\times 6}$ is the Jacobian matrix of the right foot with respect to the hip. Finally, substituting (46), (47) and (48) into the torque equation related to the right leg in (1) leads to

$$\begin{aligned}\vec{\tau}_r &= (H_r - K_r\tilde{R}^{-1}Q_r)(R_0 J_r)^{-1}(\ddot{\vec{x}}_{rf,d}\\ &\quad + M_R^{-1}(-\vec{f}_r - D_R\dot{\tilde{x}}_{rf} - E_R\tilde{x}_{rf})\\ &\quad - \ddot{\vec{x}}_h - R_0\dot{J}_r\dot{\vec{x}}_{rf} - \vec{\Omega}_r) + D_r\vec{f}_r - K_r\tilde{R}^{-1}\tilde{S} + L_r.\end{aligned} \tag{49}$$

Immediately on switching from a support phase to a flight phase, the supporting foot of the biped robot does not leave off the ground. Thus, the external force vector $\vec{f}_r$ applied at the right foot is not zero until the foot takes off the ground.

Next, the impedance controller for the swinging and landing front left leg has the same mechanism as the left leg of the support phase except that the force modulation strategy is included so that the left foot does not bounce back from the ground after touch-down. In order to reduce and modulate the large reaction force at the landing foot on the ground, the desired vertical force $f_{v,d}$ is obtained from the actual vertical force f_v. Thus,

$$f_{v,d} = \begin{cases} f_v - \Delta f, & f_v > m_g + \delta,\\ m_g, & m_g - \delta \le f_v \le m_g + \delta,\\ f_v, & f_v < m_g - \delta \end{cases} \tag{50}$$

where Δf and δ denote the reduction rate and boundary value, respectively, which are used to phase down the vertical reaction force over a control period. The desired impedance model for the swinging and landing front left leg is described as the following equation:

$$M_L\ddot{\tilde{x}}_{lf} + D_L\dot{\tilde{x}}_{lf} + E_L\tilde{x}_{lf} = \vec{f}_{l,d} - \vec{f}_l \tag{51}$$

where

$$\vec{f}_{l,d} = \begin{bmatrix}0 & 0 & f_{v,d} & 0 & 0 & 0\end{bmatrix}^T$$

and $\vec{f}_{l,d}$ denotes the desired external force vector applied at the left foot. Notice that $\vec{f}_{l,d} - \vec{f}_l$ is zero when the left foot is in the air. The parameters used in the desired impedance model are determined depending on the mechanical properties of the original system. The mass and stiffness components of the impedance model for the leg are selected to be equal to those in the SLIP model which reflects specifically the mechanical properties of the biped robot. The damping coefficients are determined such that the overall system is critically damped. The impedance parameters for the hip are selected to be 2 times larger than those of the foot such that the impact shock at touch-down should be appropriately ab-

Table 1 Physical parameters of the biped robot model used in the simulations

Link	Length (cm)	Mass (kg)	Link	Length (cm)	Mass (kg)
Link 0 (waist)	20	6.0	Link 5 (ankle)	5	1.0
Link 1	5	1.0	Link 6 (foot)	15	1.5
Link 2	5	1.0	Waist-head	35	7.0
Link 3 (thigh)	30	2.5	Left arm	50	2.0
Link 4 (knee)	30	2.5	Right arm	50	2.0

sorbed and the bouncing of the foot from the ground can be prevented. Thus,

$$M_h = \text{diag}(b_0,\ b_0,\ b_0,\ b_0,\ b_0,\ b_0),$$

$$D_h = \text{diag}(d_0,\ d_0,\ d_0,\ d_0,\ d_0,\ d_0),$$

$$E_h = \text{diag}(e_0,\ e_0,\ e_0,\ e_0,\ e_0,\ e_0)$$

where $b_0 = 2m_g$ [kg] or [kgm^2], $e_0 = 2k_{leg}$ [N/m] or [Nm], and $d_0 = 2\sqrt{b_0 e_0}$. And $M_L = M_R = 1/2M_h$, $E_L = E_R = 1/2E_h$, and $D_L = D_R = \text{diag}(d_0/2,\ d_0/2,\ d_0/2,\ d_0/2,\ d_0/2,\ d_0/2)$.

6 Simulations

6.1 Simulations without modeling error

Running of a 19-DOF biped robot is simulated for the effectiveness and performance evaluation of the proposed asymmetric trajectory and impedance controller. The biped robot has a total of 19 degrees of freedom, as shown in Fig. 1. Each leg has 6 degrees of freedom, two joints at the ankle, one joint at the knee, and three joints at the hip and the upper body has 7 degrees of freedom. The specification of the biped robot model with two legs of mass 9.5 [kg] used in the simulations is listed in Table 1. The parameters used to generate the flight phase trajectories are shown in Table 2. The control period of the computer simulation is 0.002 [s].

During running, biped robots must interact iteratively with the external environment. In particular, when a foot of the freely swinging leg makes an initial contact with the ground, a large impact force may always be generated. To protect force sensors and joints from the touch-down impact force, many biped robots are equipped with some kinds of shock-absorbing elastic pads at their soles (Yamaguchi et al. 1995). The pads in the support surface are modeled as nonlinear springs and nonlinear dampers, as shown in Fig. 1. The stiffness and damping coefficient are chosen to reflect the nonlinear characteristics of the elastic pad. This nonlinear complaint model with Coulomb friction allows rotating of the foot on the ground (Marhefka and Orin 1999; Kwon and Park 2002).

In the computer simulations performed without modeling error, the biped robot runs on a flat solid ground. Figure 9 shows a stick diagram from computer simulations of a 19-DOF biped robot when the average forward speed for running is about 0.774 [m/s] with $T_f = 0.1$ [s], $T_s = 0.4$ [s], $S_t = 0.3$ [m], and $k_{leg} = 8500.0$ [N/m], as given in Sect. 4. The biped robot moves up and down with a full running cycle of about 0.5 [s] and a maximum flight height of about 0.814 [m]. The vertical height of the hip link H_z is 0.80 [m] at the moment the biped robot leaves off the ground. During support phases, the rear foot of the biped robot pushes forward its body and front leg. At the same time, the vertical rebound of the hip cause the foot to fly in the air. In Fig. 9, the peak foot clearance during flight is about 0.05 [m]. The vertical position of the foot as a function of its horizontal position would have to be altered so that it does not collide with the ground. The impedance control with the force modulation strategy and the downward movement of the body along the vertical direction make the support foot fixed on the ground until the biped robot leaves off the ground.

Figure 10 shows how the components of linear and angular momenta about the mass center of the robot in (2) vary in the flight and support phases when the magnitude of the modified angular momentum about the mass center of the

Table 2 Parameters used in the simulations

M	16.0 kg	T_f	0.08, 0.09, 1.0 s
M_1	9.5 kg	δ	50 N
M_2	9.5 kg	Δf	100 N
T_s	0.5, 0.45, 0.4 s	σ	1/12

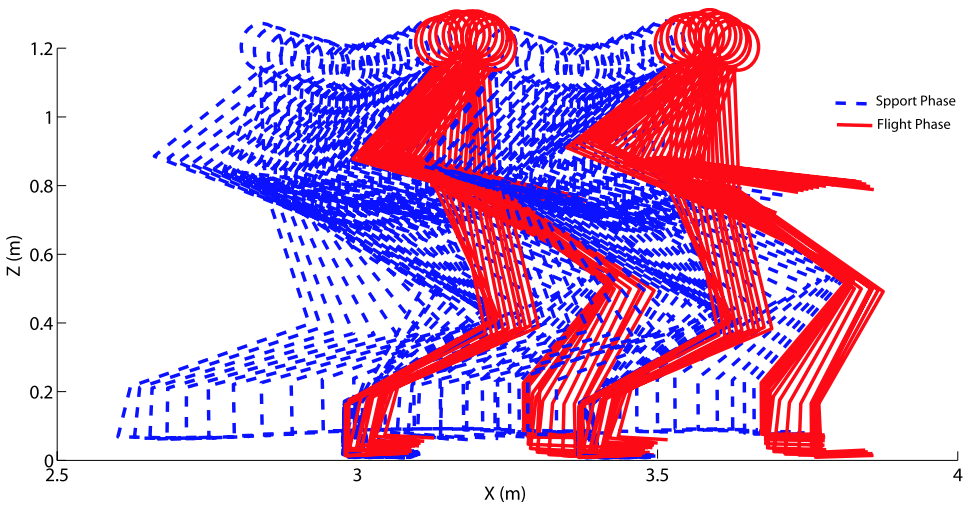

Fig. 9 Stick diagram of a biped robot with the average forward speed of 0.774 [m/s] in the sagittal plane. The maximum forward speed of the robot is about 0.9 [m/s]. The *solid lines* illustrate ballistic motions of the biped robot in the flight phase while the *dashed lines* illustrate bouncing motions of the biped robot in the support phase. The biped robot is equipped with shock-absorbing elastic pads at its soles. The depth of the pad is 0.01 [m]. The pad is compressed just after the foot makes contact with the ground. The shortest distance between the sole and the ground is about 0.005 [m]

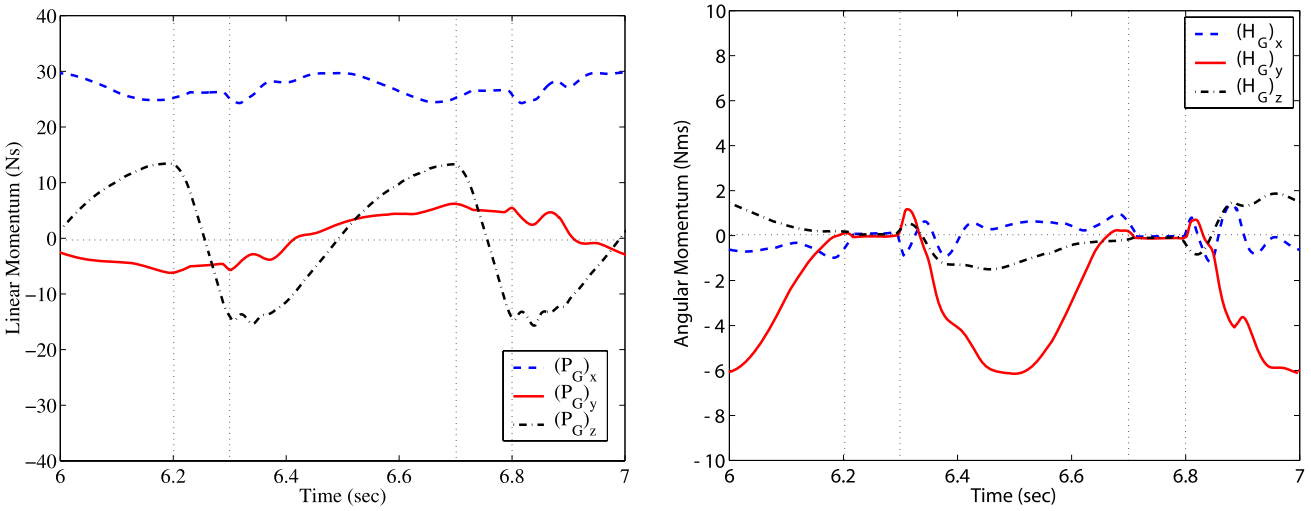

(a) Linear momentum (b) Angular momentum

Fig. 10 Linear and angular momenta. In these figures, the *vertical dotted lines* represent the instances of touch-down and lift-off

robot is set to an allowable value, i.e., $\vec{H}'_G = \vec{0}$, when $\alpha_0 = 0.02$ [Nms], $\alpha_1 = 15.0$ [m/s^2], $\alpha_2 = 0.2777$ [Nms], $\alpha_3 = 0.4421$ [Nms], $\beta_1 = 0.0159$ [Nms], and $\beta_2 = 0.0$ [Nms]. The biped robot flies in the air at times 6.215 [s] to 6.3 [s] and 6.715 [s] to 6.8 [s]. The real flight time is not equal to the desired value, since the supporting foot of the biped robot does not leave off the ground until the springs and dampers used in the compliant model restitute to their rest length after switching from a support phase to a flight phase. In these figures, the z-component of linear momentum decreases linearly due to the gravitational force and the components of angular momentum about the mass center of the robot remain unchanged within a limited scope during flight. In particular, the y-component of angular momentum about the mass center of the robot during the support phase varies within a wider range than the other components of angular momentum, since the robot rotates largely around its center of mass in the sagittal plane, if it does not change direction. Simulations of three different running patterns with respect to the flight time, T_f, as shown in Fig. 11, show that the y-components of angular momentum vary similarly. They become negative after touch-down in the support phase and recover close to almost zero before lift-off in the support phase, and then remain constant within a limited range, $|(\vec{H}_G)_y| \leq 0.4421$ [Nms], after flight.

Figure 12 shows that the ZMP stays inside the safety boundary of the footprint in the horizontal plane (X–Y plane). The ZMP oscillates from back to front after touch-down and then becomes steady in the center of the footprint, but does not exist when the two feet in the air. Figure 13 shows how the ground reaction forces change as the locomotion proceeds. The peak of the ground reaction forces felt

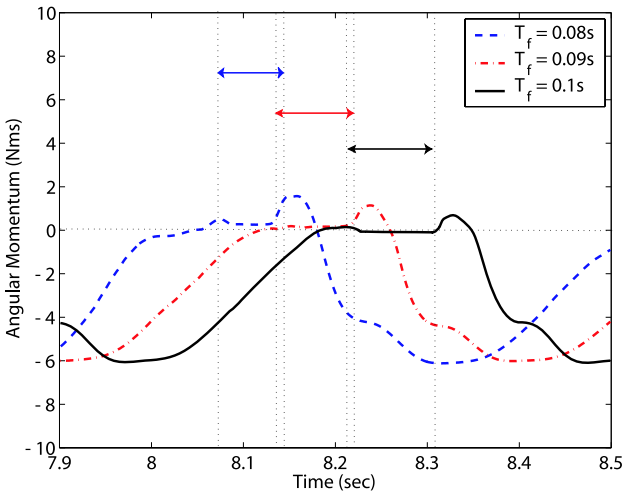

Fig. 11 y-components of angular momentum according to three different running patterns. First, the dashed line denotes the y-component of angular momentum when $T_f = 0.08$ [s]. The *dash-dotted line* denotes the y-component of angular momentum when $T_f = 0.09$ [s]. The *solid line* denotes the y-component of angular momentum when $T_f = 0.1$ [s]. The duration of the support phase, $T_s = 0.4$ [s], is all the same

at a supporting foot when times 6.3 [s] and 6.32 [s] in the initial stage of the support phase is due to the fact that the supporting foot starts to support the total weight of the biped robot. The peak of the force at the supporting foot is reduced drastically according to the desired impedance characteristics. As a result, part (b) of Fig. 10 and Fig. 12 show that the running stability conditions are satisfied.

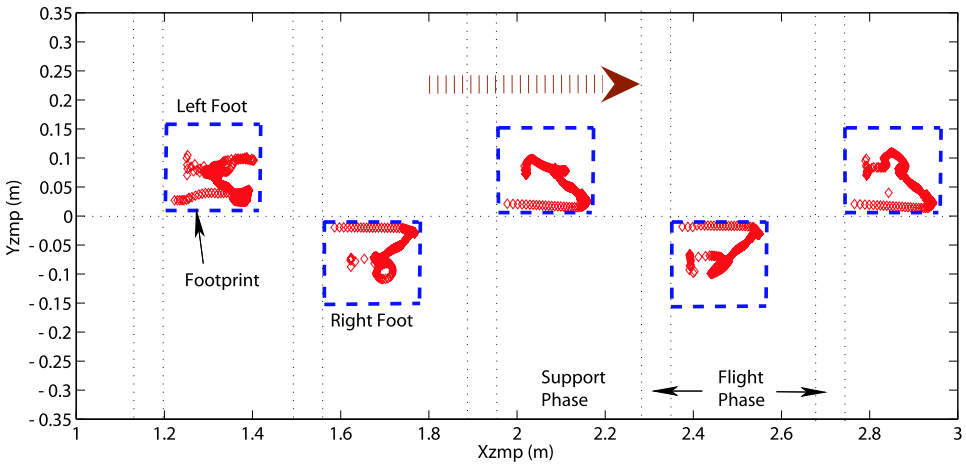

Fig. 12 ZMP trajectory in the horizontal plane (X–Y plane). The rectangles denote footprints

6.2 Gait transitions

The developed strategy was tested in case of transiting purposely gaits. An asymmetric running pattern including a gait transition between walking and running has been simulated. The locomotion parameters are given as follows:

Walking pattern

– $H_z = 0.8$ [m], $Stride = 0.3$ [m], and $Period = 0.1$ [s].

Running pattern

– $H_z = 0.8$ [m], $T_f = 0.1$ [s], $T_s = 0.4$ [s], $S_t = 0.3$ [m], $k_{leg} = 8500.0$ [N/m], and $\vec{H}'_G = \vec{0}$.

Initially, the biped robot stands still with its two feet on the ground. Then it lifts its left foot in the sagittal plane and starts moving forward along the desired trajectory at the average forward speed of 0.3 [m/s]. A transition between walking and running occurs after 6 steps, and the biped robot starts running forward at the average forward speed of 0.774 [m/s]. After 16 running cycles, a transition between running and walking occurs again, and the biped robot starts walking forward at the average speed of 0.3 [m/s].

Figure 14 illustrates the phase portraits of the position and velocity of the hip link including walk to run gait and run to walk gait transitions. First, the graph (a) of Fig. 14 shows that the hip link in the X-axis direction moves like an inverted-pendulum in both walking and running, even though two gaits have large differences in the period and magnitude of the oscillation. The graph (b) of Fig. 14 shows the lateral swinging motion of the hip link in a clock-wise fashion. The graph (c) of Fig. 14 shows the vertical bouncing motion of the hip link in a clock-wise fashion. The inner point describes that the hip link is fixed at a constant height during normal walking, and the outer distorted circles describe the vertical bouncing motion of the hip link during normal running. The curved-lines connecting the inner point

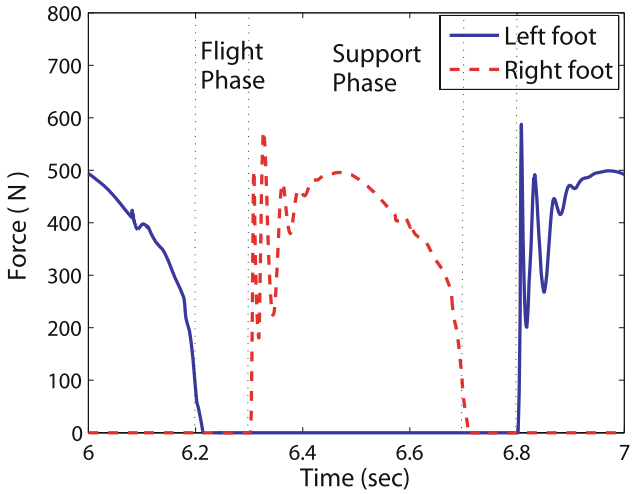

Fig. 13 Vertical reaction forces exerted on both feet. The ground reaction force reaches about twice the total weight of the biped robot at times 6.3 [s] and 6.32 [s] and then is reduced drastically

to the outer distorted circles describe the vertical oscillations of the hip link during gait transitions.

Next, a transition between two steady running patterns was considered to prove the effectiveness of the developed strategy for running. The locomotion parameters with respect to two running patterns are chosen as follows:

Running pattern 1

– $V_{xf} = 0.6$ [m/s], $H_z = 0.8$ [m], $T_f = 0.08$ [s], $T_s = 0.5$ [s], $S_t = 0.3$ [m], $k_{leg} = 8500.0$ [N/m], and $\vec{H}'_G = \vec{0}$.

Running pattern 2

– $V_{xf} = 0.7$ [m/s], $H_z = 0.8$ [m], $T_f = 0.09$ [s], $T_s = 0.45$ [s], $S_t = 0.3$ [m], $k_{leg} = 8500.0$ [N/m], and $\vec{H}'_G = \vec{0}$

where the flight time of the pattern 2 is longer more than that of the pattern 1 while the duration of the support phase for the pattern 1 is longer. Hence, the running speed from the pattern 1 to the pattern 2 is increased by about 17 percent.

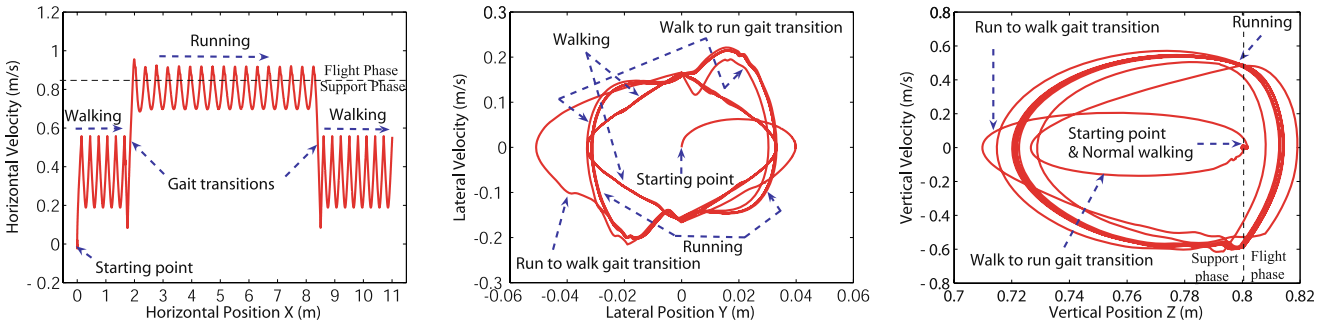

Fig. 14 Phase plots of the hip link: walk to run gait and run to walk gait transitions. Each diagram represents the reciprocal relationship between the position and velocity of the hip link. Note that position is plotted on the abscissa, velocity is on the ordinate, and the action advances in a clockwise direction in (**b**) and (**c**). The starting point indicates the starting spot from rest

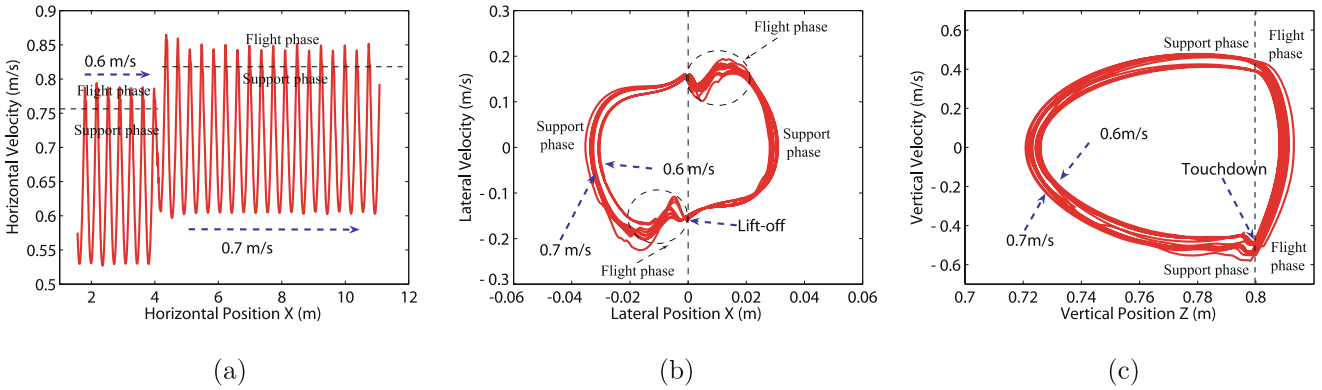

Fig. 15 Phase plots of the hip link: a transition between two steady running patterns. Each diagram represents the reciprocal relationship between the position and velocity of the hip link. Note that position is plotted on the abscissa, velocity is on the ordinate, and the action advances in a clockwise direction in (**b**) and (**c**)

The transition between the pattern 1 and the pattern 2 occurs during the support phase such that at the end of that support phase the necessary initial conditions for the flight phase of the pattern 2 are reached. Figure 15 shows the phase portraits of the position and velocity of the hip link including a transition between two steady running patterns. After the flight phase of the pattern 1, the average forward speed of the robot is switched gradually from 0.6 [m/s] to 0.7 [m/s] during the following support phase, and the steady-state running for the pattern 2 at the average forward speed of 0.7 [m/s] is attained before lift-off. Each plot shows that the phase portrait oscillates largely just after touch-down and then is converged into a periodic orbit.

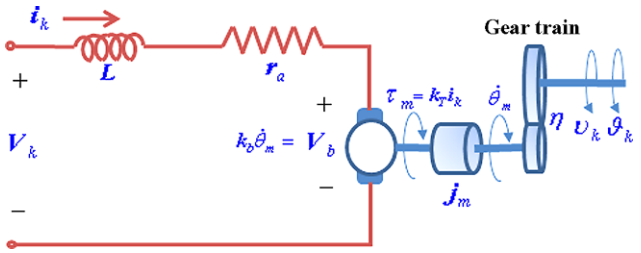

Fig. 16 Model of a DC motor in series with a gear train. τ_m and θ_m denote the torque and angular velocity of a motor, respectively. V_b and L denote the back electro-motive-force voltage and inductance of a motor, respectively

6.3 Actuator limits

Motion performances of a biped robot strongly depend on performances of the actuators. Thus, the actuator dynamics and limits are typically limiting constraints in running locomotion. In general, permanent magnet DC motors in series with a gear train are used as the actuators for a multi-DOF humanoid robot (Nagasaki et al. 2003; Spong and Vidyasagar 1989; Arikawa and Mita 2002). The actuator dynamics about the armature voltage V_k and armature current i_k of k-th revolute joint can be derived from the simplified model of a DC motor in series with a gear train,

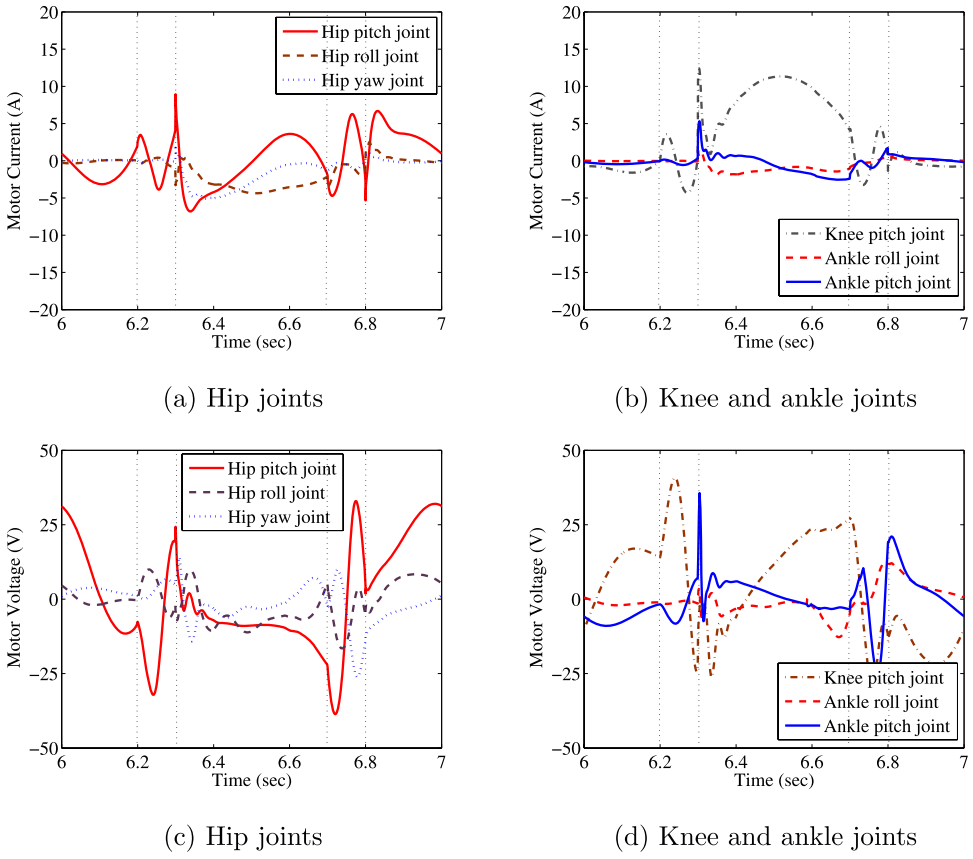

Fig. 17 Motor current and voltage at each joint of the right leg for running

(a) Hip joints (b) Knee and ankle joints

(c) Hip joints (d) Knee and ankle joints

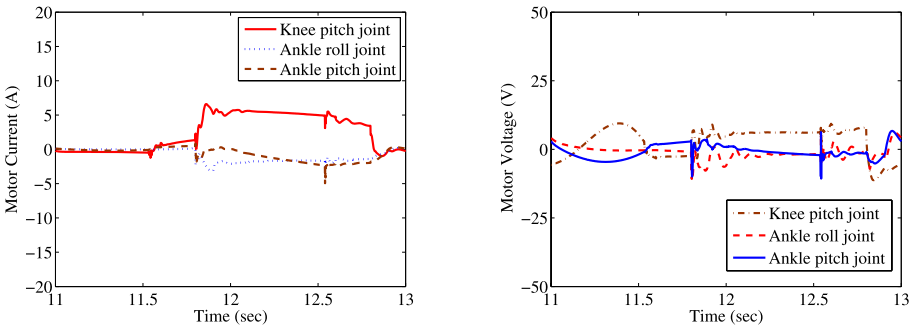

Fig. 18 Motor current and voltage at each joint of the right leg for walking

(a) Motor current at knee and ankle joints (b) Motor voltage at knee and ankle joints

as shown in Fig. 16. Thus,

$$i_k = \frac{j_m}{\eta k_T}\ddot{\vartheta}_k + \frac{b_m}{\eta k_T}\dot{\vartheta}_k + \frac{\eta}{k_T}\upsilon_k,$$
$$V_k = \frac{j_m r_a}{\eta k_T}\ddot{\vartheta}_k + \left(\frac{b_m r_a}{\eta k_T} + \frac{k_b}{\eta}\right)\dot{\vartheta}_k + \frac{\eta r_a}{k_T}\upsilon_k, \quad (52)$$
$$k = 1, 2, \ldots, n$$

where η denotes the gear reduction ratio (1/110, 1/120, 1/128, 1/160) which is one of the important design parameters. It is assumed that the inductance in the armature circuit is neglected and the gear train transmits the power unchanged. j_m denotes the sum of the DC motor and gear train inertias; b_m denotes the sum of viscous-friction coefficients of the DC motor and gear; k_T, k_b, and r_a denote the torque constant, back electro-motive force constant, and armature resistance of the motor, respectively; $\dot{\vartheta}_k$ and υ_k denote the angular velocity and torque of k-th joint, respectively. The parameters of all actuators are based on the commercial DC motor (Maxon Motor co., http://www.maxonmotor.com). Thus, j_m: $(0.0134+0.054)\times 10^{-3}$ [kgm^2], b_m: 2.68042×10^{-5} [Nms], k_T: 0.0604 [Nm/A], k_b: 0.0603 [Vs/rad], and r_a: 1.16 [Ω]. The maximum torque is mainly determined by the maximum current i_{max} which is restricted

by the capability of the DC motor driver while the maximum speed is mainly determined by the maximum voltage V_{max} which is dependent on the power supply voltage. $i_{max} = 20.0$ [A] and $V_{max} = 48.0$ [V] from the specification of commercial motor drivers are used to evaluate the actuator limits in the simulation. Figure 17 shows that the motor current and voltage needed for the right leg for running does not exceed the actuator limits. The maximum motor current needed in running is about 1.5 times larger than that in walking, as illustrated in Figs. 17 and 18. In particular, the knee pitch joint needs relatively large motor current because it must absorb the large vertical force caused by an impulsive collision at every footfall and make the biped robot rebound into the air. Also, it needs high motor voltage in order to make a front leg move into the desired landing position during the flight phase.

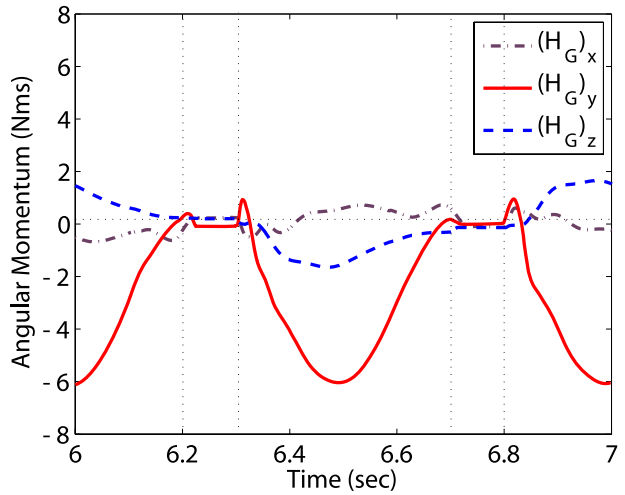

Fig. 19 Components trajectories of the angular momentum at the mass center of the biped robot. The control system has a deviation of ± 25 percent in the parameters of links

6.4 Simulation with parametric modeling error

The proposed method was successful in the simulations including the 6-DOF contact model with static friction coefficient $\mu_s = 0.5$. In addition, the robustness test of the proposed method is performed with respect to parametric modeling error. A deviation of ± 25 percent in the masses and inertias of links between the simulation model and the control model used in the impedance controller is introduced, since accurate values of the parameters of links are typically unknown even to manufacturers of a robot, and determining the parameters from computer design tools and experimental measurements is generally difficult. It is important to note that the parametric modeling error leads to errors in the configuration and speed of the robot at the instance of touch-down and also generates the large impact force at the supporting foot.

Figure 19 shows how the components of the angular momentum at the mass center vary, when the control system for running of a biped robot has the parametric modeling errors. A biped robot walks along the desired trajectory with the forward walking speed of 0.3 m/s. After a gait transition between walking and running, the biped robot runs with a average forward speed of 0.774 [m/s]. The biped robot flies in the air at times 6.23 [s] to 6.3 [s] and 6.73 [s] to 6.8 [s]. Even though the duration of the flight phase becomes far shorter than the planned value, the components of the angular momentum at the mass center of the biped robot are kept constant within an allowable range during flight. The allowable range of the angular momentum which is defined according to the desired motion patterns of the support phase is $|(\vec{H}_G)_y| \leq 0.4421$ [Nms]. Figure 20 shows phase-plane evolutions of the position and velocity of the hip link bouncing and swinging with the average speed of 0.774 [m/s], after a walk to run gait transition. Even though a marked deviation from normal running occurs just after the gait transition, the plots (a)–(c) of Fig. 20 indicate that each phase portrait converges into periodic orbits.

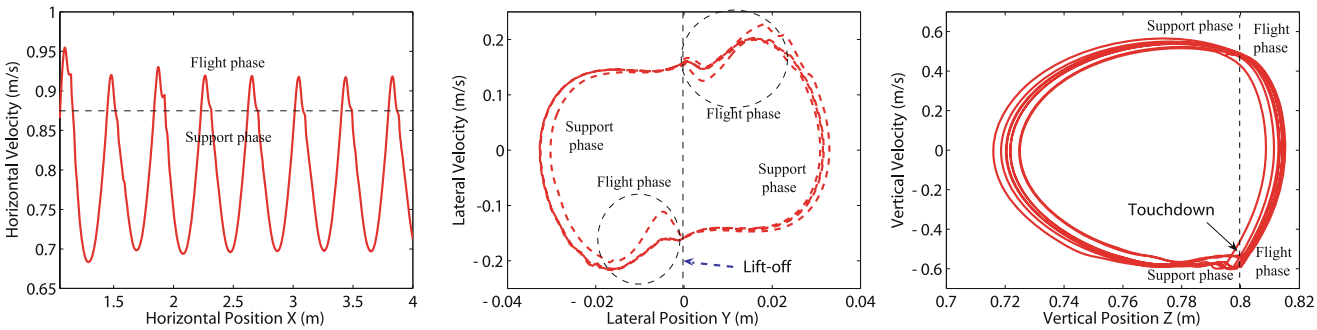

Fig. 20 Phase plane diagrams of the hip link bouncing and swinging after a walk to run gait transition. The control system has a deviation of ± 25% in the parameters of links. Each diagram represents the reciprocal relationship between the position and velocity of the hip link

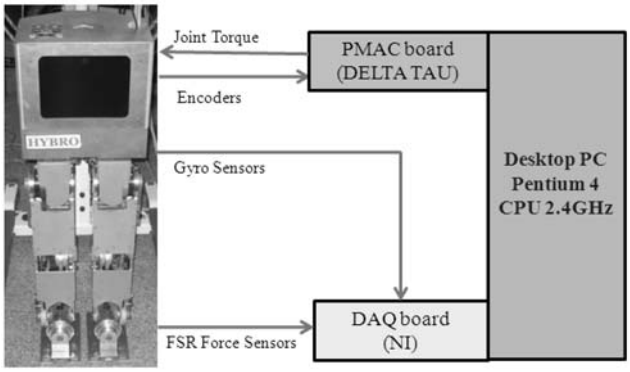

Fig. 21 A 12-DOF biped robot and control architecture for running experiments. The control system consists of a PMAC motor control board, a DAQ board, and a Desktop PC. The DAQ board handles analog signal output from FSR force sensors (pressure sensors) and Gyro sensors

Table 3 Physical parameters of the biped robot model used in the simulation and experiment

Link	Length (cm)	Mass (kg)
Link 0 (waist-upperbody)	18	15.9518
Link 1	0.1235	1.8460783
Link 2	0.0	0.0
Link 3 (thigh)	0.26	2.9653
Link 4 (shin)	0.255	3.4435
Link 5 (ankle)	0.0	0.0
Link 6 (foot)	0.08565	1.2693

Table 4 Parameters used in the simulation and experiment

M	16.0 kg	T_f	0.06 s
M_1	9.5 kg	δ	50 N
M_2	9.5 kg	Δf	100 N
T_s	0.46 s	σ	1/12

7 Running experiments

In order to verify that the proposed method is versatile enough for biped robots different in kinematic structures, running simulations and experiments are done with a 12-DOF biped robot of mass 35.0 [kg] without both arms, as shown in Fig. 21. Each leg of the biped robot has 6 degrees of freedom, two joints at the ankle, one joint at the knee, and three joints at the hip. The specification of the biped robot model is listed in Table 3. The leg weighs 9.5 [kg] due to permanent magnet DC motors in series with a gear train. It is important to note that this robot model without both arms is different from the link length of the robot model used in the previous sections.

As a counterweight, swinging both arms helps balance the upright body while running. At the same time, moving the upper limbs back and forth rhythmically with the legs prevents the supporting foot from rotating about the vertical axis. Without swinging arms, the swinging motion of two legs with relatively heavy mass generates a rotation of the upper body and legs around the vertical axis. In order to compensate the yaw moment during a support phase, the hip of the biped robot is controlled to rotate about the vertical axis synchronously with the action of the swing leg. Hence,

$$(\dot{\bar{\omega}}_h^0)_z = \frac{2M_2|Y_{sf}|}{I_{hz}}\ddot{X}_{sf} \tag{53}$$

where I_{hz} denotes the inertia moment of the hip about the vertical axis with respect to the absolute coordinates.

The control period is set to 0.00264 [s] since it takes about 0.00164 [s] to capture data from force sensors and Gyro sensors and about 0.001 [s] to calculate input torques from the control method. When comparing to the data capture time, the calculation time for the control input is considerably short, which makes the control method applied online.

The vertical height of the hip is 0.7242 [m] with knee stretched fully. The allowable ranges of the locomotion parameters for a support phase are chosen as $H_{z,min} = 0.61$ [m], $H_{z,max} = 0.71$ [m], $S_{t,min} = 0.1$ [m], and $S_{t,max} = 0.2$ [m]. The locomotion parameters are determined by the same method given in Sect. 4. Thus, $T_s = 0.46$ [s], $S_t = 0.15$ [m], $H_z = 0.693$ [m] and $k_{leg} = 7500.0$ [N/m]. The parameters used in the fight phase trajectories are given in Table 4. Figures 22 and 23 show graphs of the angular momentum and the ZMP during normal running in the simulation of the 12-DOF biped robot, respectively. As a result, these plots show that they does not move out of the predefined stability region.

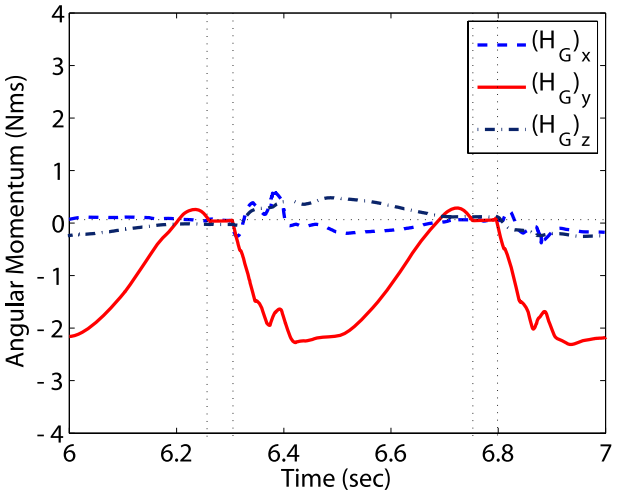

Fig. 22 Curves of angular momentum at the mass center in the simulation of the 12-DOF biped robot

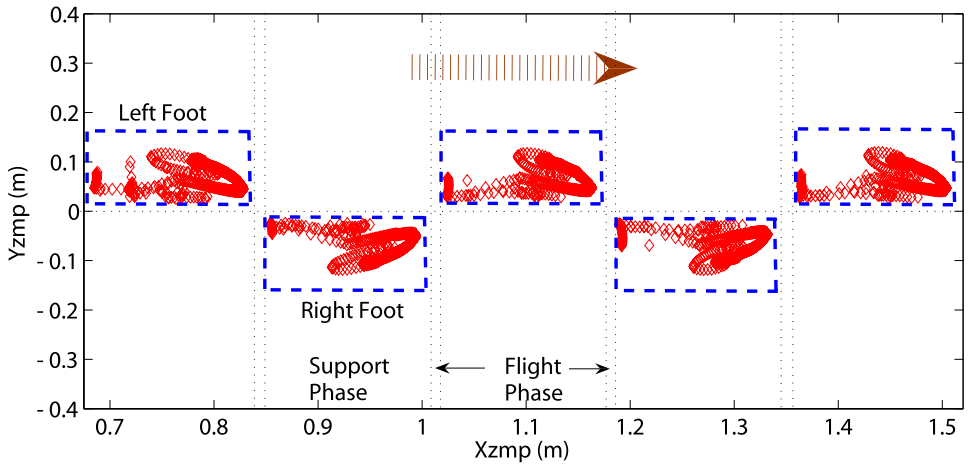

Fig. 23 ZMP trajectory in the simulation of the 12-DOF biped robot. The *rectangles* denote footprints in the horizontal plane (X–Y plane)

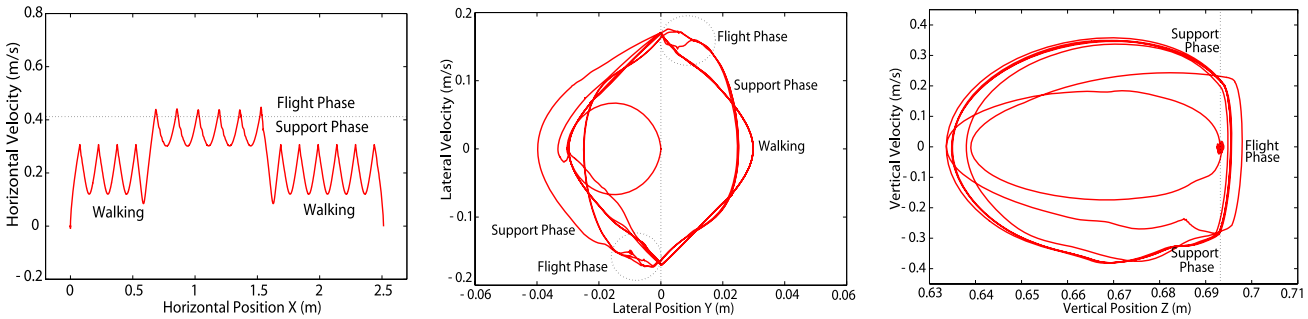

(a) (b) (c)

Fig. 24 Phase plane diagrams of the hip link bouncing and swinging in the simulation of the 12-DOF biped robot. Each diagram represents the reciprocal relationship between the position and velocity of the hip link. Note that position is plotted on the abscissa, velocity is on the ordinate, and the action advances in a clockwise direction in (**b**) and (**c**)

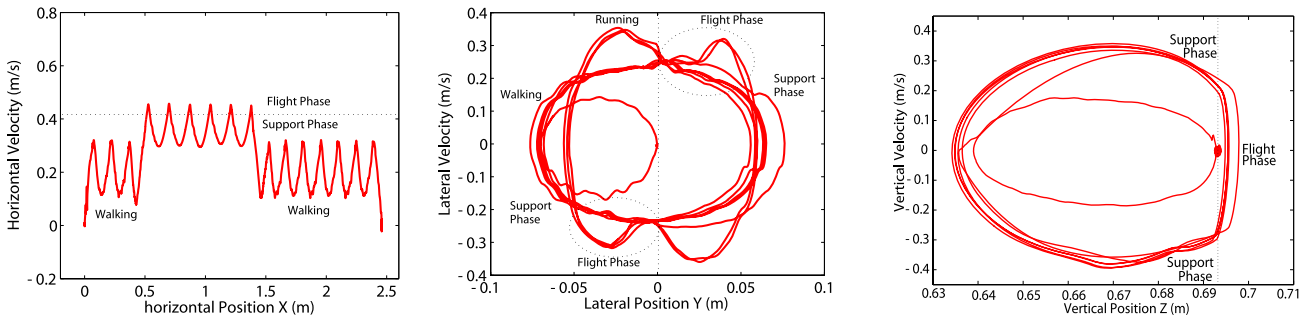

(a) (b) (c)

Fig. 25 Phase plane diagrams of the hip link bouncing and swinging in the experiment of the 12-DOF biped robot. Each diagram represents the reciprocal relationship between the position and velocity of the hip link. Note that position is plotted on the abscissa, velocity is on the ordinate, and the action advances in a clockwise direction in (**b**) and (**c**)

Figure 24 shows the phase plane diagrams of the hip in the simulation of the 12-DOF biped robot. The vertical height of the hip link H_z is 0.693 [m] at the moment the biped robot leaves off the ground with the maximum flight height of about 0.698 [m]. The peak foot clearance is about 0.04 [m], as the robot runs at the average speed of about 0.3359 [m/s]. In these phase portraits, the hip of the robot bounces and swings along the forward velocity which

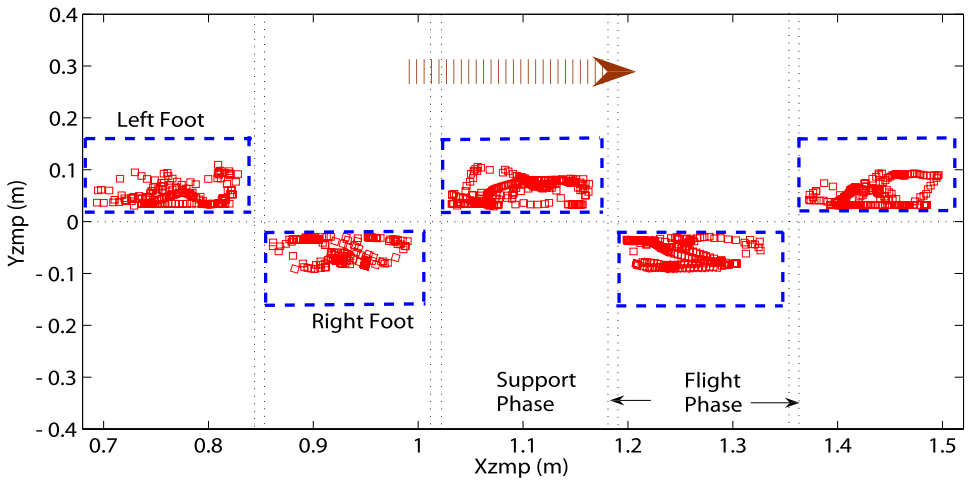

Fig. 26 ZMP trajectory in the experiment of the 12-DOF biped robot. The *rectangles* denote footprints in the horizontal plane (X–Y plane)

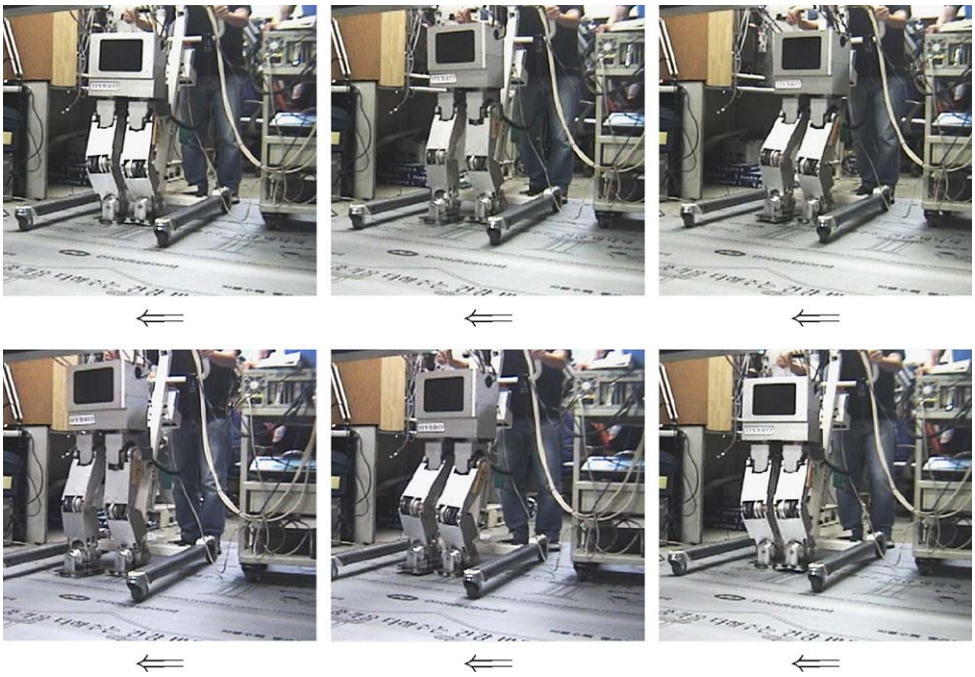

Fig. 27 Consecutive snapshots of the 12-DOF biped robot with running gaits. Vinyl flooring is used to protect the FSR force sensors and harmonic drivers from the impact force exerted on the foot. The snapshots are spaced at 0.1 [s]

is chosen to be suited to the link length and mass of the robot model.

In the experiments, encoders were used to measure joint angles and velocities of revolute joints. In order to obtain the velocity and acceleration of the hip link, the measured joint angles and velocities are differentiated and double-differentiated, respectively, by a digital differentiating filter. However, the need to differentiate the velocity numerically to find the acceleration greatly amplifies whatever noise is present. The joint encoders are easily contaminated with noise in harsh environments. Therefore, Kalman estimators are used to estimate the optimum steady state position, velocity, and acceleration of a biped robot moving with a constant acceleration perturbed by a zero mean plant noise which accounts for maneuvers or other random factors (Ramachandra 2000). Similarly, the orientation of the robot is estimated from the raw voltage outputs of Gyro sensors using Kalman estimators.

Figure 25 shows phase-plane evolutions of the hip link bouncing and swinging in the flight and support phases for a average speed of about 0.3359 [m/s]. Initially, the biped robot stands still with its feet on the ground. Then the left foot is lifted first and the biped robot starts to walk forward along the desired trajectory at the average forward speed of 0.1776 [m/s]. The speed transition between walking and running occurs after 3 steps, and the biped robot starts running forward at the average speed of 0.3359 [m/s]. After 6 running cycles, the speed transition between walking and running occurs, and the biped robot starts to walk forward at the average speed of 0.1776 [m/s]. After 7 steps, it comes

to a stop and then stands with its two feet on the ground. When the vertical force measured from force sensors becomes larger than about m_g g/100.0 [N] after touchdown, the control system of the biped robot has a phase switch from a flight phase to a support phase. This is due to the fact that it is difficult to measure exactly the instance of touchdown.

A supporting leg of the robot is flexible due to elastic deformations of links and revolute joints, even though the robot was built for experimental verification of the dynamic simulations. The revolute joint is actuated by a permanent magnet DC motor-pulley-single stage timing belt-pulley-harmonic driver system. The flexibility of the supporting leg is briefly modeled into an inverted pendulum model with a rotational spring. If the stiffness of the rotational spring is determined experimentally, the support phase trajectory of the hip link is modified to compensate the elastic deformation of the supporting leg. When comparing the phase portrait of Fig. 25(b) to the corresponding graph of Fig. 24(b), it can be seen that the hip link of the robot is controlled to move within a wider range than that in the simulations. In addition, the force of friction slows the revolute joint down as it rotates. The effect of the joint friction is determined experimentally, and then it is added to (52).

The ZMP is calculated using the force data that are measured by six pressure sensors mounted at the sole of the robot during the support phase, as given in Appendix A. Figure 26 shows the ZMP trajectory in the horizontal plane (X–Y plane). The ZMP does not move from the rear edge to the fore edge of the support foot, since the robot flies in the air without toe joints, as can be seen on the front area of the footprint in the plot. The ZMP stays inside the boundary of the footprint in the horizontal plane (X–Y plane) as the locomotion proceeds. Figure 27 shows consecutive snapshots of the 12-DOF biped robot running without both arms.

8 Conclusions

Symmetric running makes control of the robot simple and easy. In the case of biped robots with relatively heavy legs and arms, large deviations from symmetry occur frequently in the instances of touch-down and lift-off. The control system requires a lot of works to eliminate the large error and to recover to the normal and symmetric pattern. Such recovery works may increases energy consumption. It is effective to exploit asymmetry that can provide balanced steady-state running patterns and reduce energy consumption. We proposed an trajectory generation method to make the biped robot run asymmetrically. The method was achieved by the asymmetric motion of the hip link and two legs based on the SLIP-like motion as well as the approximated running model with two legs. The asymmetric motion reduces energy consumption so that joint power for running of the robot does not exceed the allowable limit of the commercial actuator and driver system. It did not lead to the least energy consumption, but to the locally-optimized energy consumption.

The trajectory generation strategy was implemented on a model with heavy articulated legs, arms and vertically placed upper body with its center of mass which is not located at the hip link. During flight, the angular momentum is conserved. If the feet are controlled to move to a desired position during flight, the upper body with its larger mass and inertia in comparison with the legs inevitably rotates around the mass center. Control of the body rotation was accomplished by using the approximated running model and simplified equations of the linear and angular momenta. The essential characteristics in biped running could be captured with the approximated running model with two springless legs in order to avoid the rotation of the upper body during flight. Applying properly chosen values for the angular momentum to the running model clearly resulted in good performance.

The running stability criterion based on the ZMP and the angular momentum was used to ensure that the generated asymmetrical trajectories guarantee a high level of dynamical postural stability for the robot. The ZMP criterion is quantified by the distance of the ZMP to the boundaries of a stability region so that one step does not cause the system to tip over entirely before the next step. In the case of the angular momentum, it cannot be manipulated once the flight phase begins. The allowable range of angular momentum at the mass center of the biped robot for flight was determined according to the desired trajectory of the support phase after touch-down or before lift-off. The proper value of the angular momentum chosen in the predefined stability region was reached just before lift-off.

The trajectory generation strategies were developed with respect to two different types of biped robots. The effectiveness of the developed strategies was verified by a variety of computer simulations, showing that they are effective regardless of the kinematic differences of the two biped robots. Experiments indicated that the 12-DOF biped robot balanced while running at the average forward speed of about 0.3359 [m/s] on the Vinyl flooring. An interesting aspect of these methods is that the locomotion parameters for the asymmetric pattern is determined to be properly matched to kinematic structure and locomotion condition of the robot. The computation time needed for generating feasible trajectories and implementing the impedance control is relatively short. The methods can be applied to the experiments online.

In general, quantitative measures of the angular momentum at the mass center of the biped robot can be obtained

from force data measured by foot force sensors at the moment of lift-off combined with motion data measured by Gyro sensors and acceleration sensors after lift-off. However, it is difficult to quantify the angular momentum exactly online due to kinematic modeling errors and properly uncompensated sensor errors. As a future work, further continuing studies are required to estimate the angular momentum online and to find the correct amount of the angular momentum required for the style of flight. In addition, we will study an online control of the measured angular momentum for running of biped robots on uneven surface.

Appendix A: Zero moment point (ZMP)

The ZMP is simply the center of the pressure (COP), normal to the sole, applied at the soles by the ground. The resultant ground normal force can be represented by a single force at that point without any associated moment. By definition, the ZMP should remain inside the convex hull of the foot-support in the single support phase. Under the assumption that no external force nor external moment exists except at the soles, its relationship with dynamic variables of the biped robot can be also easily obtained as the following equation:

$$\begin{aligned} X_{\text{zmp}} &= \frac{\sum_{k=1}^{n} m_k\left(-\ddot{x}_k z_k + (\ddot{z}_k + g)\, x_k\right) - I_{ky}\ddot{\phi}_{ky}}{\sum_{k=1}^{n} m_i\,(\ddot{z}_k + g)} \\ &= \frac{-(\dot{\vec{H}}_0)_y + \sum_{k=1}^{n}(m_k g x_k)}{\sum_{k=1}^{n} m_k\,(\ddot{z}_k + g)}, \\ Y_{\text{zmp}} &= \frac{\sum_{k=1}^{n} m_k\left(-\ddot{y}_k z_k + (\ddot{z}_k + g)\, y_k\right) + I_{kx}\ddot{\phi}_{kx}}{\sum_{k=1}^{n} m_k\,(\ddot{z}_k + g)} \\ &= \frac{(\dot{\vec{H}}_0)_x + \sum_{k=1}^{n}(m_k g y_k)}{\sum_{k=1}^{n} m_k\,(\ddot{z}_k + g)} \end{aligned} \tag{54}$$

where

$$(\vec{H}_0)_x = \sum_{k=1}^{n}(-m_k \dot{y}_k z_k + m_k \dot{z}_k y_k + I_{kx}\dot{\phi}_{kx}),$$

$$(\vec{H}_0)_y = \sum_{k=1}^{n}(m_i \dot{x}_k z_k - m_k \dot{z}_k x_k + I_{ky}\dot{\phi}_{ky}),$$

and g is the gravity, i.e., 9.8 [m/s^2]. Each element of the linear and angular momenta is derived using the Newton's law and (54).

$$\begin{aligned} x &: (\dot{\vec{P}}_0)_x = \sum_{k=1}^{n} m_k \ddot{x}_k = F_x \\ y &: (\dot{\vec{P}}_0)_y = \sum_{k=1}^{n} m_k \ddot{y}_k = F_y \\ z &: (\dot{\vec{P}}_0)_z = \sum_{k=1}^{n} m_k \ddot{z}_k = F_z - \sum_{k=1}^{n} m_k g \\ \Phi_x &: (\dot{\vec{H}}_0)_x = Y_{\text{zmp}} \cdot F_z - \sum_{k=1}^{n} m_k g y_k \\ \Phi_y &: (\dot{\vec{H}}_0)_y = -X_{\text{zmp}} \cdot F_z + \sum_{k=1}^{n} m_k g x_k \\ \Phi_z &: (\dot{\vec{H}}_0)_z = X_{\text{zmp}} F_y - F_x Y_{\text{zmp}} \end{aligned} \tag{55}$$

where F_x, F_y and F_z are the contact forces exerted on a supporting foot. I_{kx}, and I_{ky} denotes the inertia moments of k-th link represented by the absolute coordinates in the X-axis, and Y-axis, respectively. These equations state that each element of the rate of change in angular momentum with respect to the absolute coordinates is directly related to the ZMPs, contact forces, and gravitational force. In general, the ZMPs are directly measurable with a force/torque sensor installed at the ankle, or pressure sensors installed at the sole. In this paper, six pressure sensors located at the four corners and middle of a foot in the shape of a square are used, since they are light, thin and reliable even if a variety of sensors including 6-dof force/torque sensors, load cells and strain gauges can be employed under the foot to obtain the ZMP information (Li et al. 1991; Erbatur et al. 2002).

Appendix B: Inverted pendulum model (IPM)

The IPM assumes that the total mass of the body is concentrated at the hip (base link) as an inverted pendulum (Park and Kim 1998). From this model, we can easily derive the moment equation about the ZMP.

$$\vec{r}_h \times (m_g \ddot{\vec{r}}_h) = \vec{r}_h \times (m_g \vec{g}) \tag{56}$$

where $\vec{r}_h = [X\ Y\ Z]^T$ denotes the position of the hip link, and m_g is the mass of the biped robot excluding the swing leg. Equation (56) is described by the following equation:

$$m_g \begin{bmatrix} Y\ddot{Z} - Z\ddot{Y} \\ Z\ddot{X} - X\ddot{Z} \\ X\ddot{Y} - Y\ddot{X} \end{bmatrix} = m_g \begin{bmatrix} -gY \\ gX \\ 0 \end{bmatrix}. \tag{57}$$

Assuming that $Z = H_z = \text{constant}$ (the height of the hip link from the ground) in (56),

$$\ddot{X} - \omega^2 X = 0, \qquad \ddot{Y} - \omega^2 Y = 0 \tag{58}$$

where $\omega = \sqrt{g/H_z}$. The solutions of (58) are

$$X(t) = C_1 e^{\omega t} + C_2 e^{-\omega t}, \qquad Y(t) = D_1 e^{\omega t} + D_2 e^{-\omega t} \quad \text{for } 0 \le t \le T_s \tag{59}$$

where

$$C_1 = \frac{1}{2}\left(X(0) + \frac{1}{\omega}\dot{X}(0)\right), \qquad C_2 = \frac{1}{2}\left(X(0) - \frac{1}{\omega}\dot{X}(0)\right),$$
$$D_1 = \frac{1}{2}\left(Y(0) + \frac{1}{\omega}\dot{Y}(0)\right), \qquad D_2 = \frac{1}{2}\left(Y(0) - \frac{1}{\omega}\dot{Y}(0)\right),$$

and variables $X(0)$ and $\dot{X}(0)$ are the initial position and the initial velocity in the X-axis direction, respectively, while variables $Y(0)$ and $\dot{Y}(0)$ are the initial position and the initial velocity in the Y-axis direction, respectively. In addition, T_s is the duration of the support phase. It is important to note that an assumption is that the height of the hip link from the ground is kept constant to get the analytical solution without difficulty. Such approximation will be valid since the period of a support phase is relatively short.

If the biped robot has a steady, symmetric and repeatable pattern, the following repeatability conditions should be satisfied.

$$\begin{aligned} &X(0) = -X(T_s), \qquad \dot{X}(0) = \dot{X}(T_s), \\ &Y(0) = Y(T_s), \qquad \dot{Y}(0) = -\dot{Y}(T_s). \end{aligned} \tag{60}$$

The initial velocities of the hip link can be found by (60) and (59). Thus,

$$\dot{X}(0) = \frac{1+e^{\omega T_s}}{1-e^{\omega T_s}}\omega X(0), \qquad \dot{Y}(0) = \frac{1-e^{\omega T_s}}{1+e^{\omega T_s}}\omega Y(0). \tag{61}$$

Appendix C: Spring loaded inverted pendulum model (SLIPM)

A spring loaded inverted pedulum model which is approximatedly embedded into a biped robot in the sagittal plane is shown in Fig. 4 (Papadopoulos and Cherouvim 2004). It is assumed that the total mass of the body and swing leg is concentrated at the hip (base link) and that the supporting leg is a massless spring with a nominal length l_0. In the figure, the leg stiffness k_{leg} is the stiffness of a linear spring and S_t is the stride of the biped robot in the support phase.

The equations of motion for this model in the sagittal plane using $\vec{r}_h \times (m_g \ddot{\vec{r}}_h) = \vec{r}_h \times (m_g \vec{g})$ in (56) and $m_g \ddot{\vec{r}}_h = m_g \vec{g} + k_{leg}(\vec{r}_h(0) - \vec{r}_h)$ is derived as the following equations:

$$\begin{aligned} &m_g l^2 \ddot{\varphi}\cos^2\psi + 2m_g l\dot{l}\dot{\varphi}\cos^2\psi - 2m_g l^2\dot{\psi}\dot{\varphi}\cos\psi\sin\psi \\ &\quad - m_g g l\sin\varphi\cos\psi = 0, \\ &m_g l^2\ddot{\psi} + 2m_g l\dot{l}\dot{\psi} - m_g g l\cos\varphi\sin\psi \\ &\quad + m_g l^2\dot{\varphi}^2\cos\psi\sin\psi = 0, \\ &m_g\ddot{l} - m_g l\dot{\psi}^2 - m_g l\dot{\varphi}^2\cos^2(\psi) + k_{leg}(l-l_0) \\ &\quad + m_g g\cos\varphi\cos\psi = 0 \end{aligned} \tag{62}$$

where $\vec{r}_h(0)$ denotes the initial position of the base link, and the leg forms an angle φ with the vertical axis in the sagittal plane and an angle ψ with the vertical axis in the frontal plane while the length of the leg at any moment in time is l. And $X = l\cos\psi\sin\varphi$, $Y = l\cos\psi$, and $Z = l\cos\psi\cos\varphi$. For small φ, the equations of motion in (62) can be linearized. Thus, linear mathematical models for the nonlinear equations of (62) in the neighborhood of the normal operating point $\varphi = 0$, $\psi = 0$, and $l = l_0$ are given by

$$\begin{aligned} &l_0\ddot{\varphi} - g\varphi = 0, \\ &l_0\ddot{\psi} - g\psi = 0, \\ &m_g\ddot{l} + k_{leg}(l-l_0) + m_g g = 0. \end{aligned} \tag{63}$$

The solutions of (63) are

$$\begin{aligned} &\varphi(t) = E_1 e^{\omega_1 t} + E_2 e^{-\omega_1 t}, \\ &\psi(t) = E_3 e^{\omega_1 t} + E_4 e^{-\omega_1 t}, \\ &l(t) = m_g g/k_{leg}\ \cos(\omega_2 t) + \sqrt{m_g/k_{leg}}\ \dot{l}(0)\sin(\omega_2 t) \\ &\qquad + l_0 - m_g g/k_{leg} \quad \text{for} \quad 0 \le t \le T_s \end{aligned} \tag{64}$$

where

$$E_1 = \frac{\varphi(0)}{2} + \frac{\dot{\varphi}(0)}{2\sqrt{g/l_0}}, \qquad E_2 = \frac{\varphi(0)}{2} - \frac{\dot{\varphi}(0)}{2\sqrt{g/l_0}},$$
$$\omega_1 = \sqrt{g/l_0},$$
$$E_3 = \frac{\psi(0)}{2} + \frac{\dot{\psi}(0)}{2\sqrt{g/l_0}}, \qquad E_4 = \frac{\psi(0)}{2} - \frac{\dot{\psi}(0)}{2\sqrt{g/l_0}},$$
$$\omega_2 = \sqrt{k_{leg}/m_g}, \qquad l_0 = l(0) = \sqrt{{H_z}^2 + (S_t/2)^2},$$
$$S_t = -2H_z\tan(\varphi(0)),$$

and variables $\varphi(0)$ and $\dot{\varphi}(0)$ are the initial angle and the initial angular velocity about the vertical axis in the sagittal plane, respectively. Variables $\psi(0)$ and $\dot{\psi}(0)$ are the initial angle and the initial angular velocity about the vertical axis in the frontal plane, respectively

Running is composed of a symmetric part and an asymmetric part. Symmetric running states that the two legs and body form approximately symmetric configurations with respect to a vertical axis passing through the hip during a flight phase or support phase. Asymmetric running deviates from symmetry.

C.1 Symmetric running

If the biped robot has a steady, symmetric and repeatable pattern, the following repeatability conditions should be sat-

isfied in the sagittal plane. Thus,

$$\varphi(0) = -\varphi(T_s), \qquad \dot{\varphi}(0) = \dot{\varphi}(T_s),$$
$$l(0) = l(T_s), \qquad \dot{l}(0) = -\dot{l}(T_s). \tag{65}$$

where the biped robot touches the ground at times 0 and $T_s + T_f$. Applying (65) to (64) leads to the initial velocities of the hip link at touch-down in the sagittal plane. Thus,

$$\dot{\varphi}(0) = \frac{1 + e^{\omega_1 T_s}}{1 - e^{\omega_1 T_s}} \omega_1 \varphi(0),$$
$$\dot{l}(0) = \frac{g\sqrt{m_g/k_{leg}}\sin(\omega_2 T_s)}{1 + \cos(\omega_2 T_s)}. \tag{66}$$

For symmetric running, the trajectory of the hip link (X, Z) in the sagittal plane is obtained by inserting $X(t) = l(t)\sin\varphi(t)$, $Z(t) = l(t)\cos\varphi(t)$, and (66) into (64) during a support phase.

$$\begin{aligned} X(t) &= (m_g g/k_{leg}\cos(\omega_2 t) + \sqrt{m_g/k_{leg}}\,\dot{l}(0)\sin(\omega_2 t) \\ &\quad + l_0 - m_g g/k_{leg})\sin(E_1 e^{\omega_1 t} + E_2 e^{-\omega_1 t}), \\ Z(t) &= (m_g g/k_{leg}\cos(\omega_2 t) + \sqrt{m_g/k_{leg}}\,\dot{l}(0)\sin(\omega_2 t) \\ &\quad + l_0 - m_g g/k_{leg})\cos(E_1 e^{\omega_1 t} + E_2 e^{-\omega_1 t}) \end{aligned} \tag{67}$$

for $0 \le t \le T_s$.

In the frontal plane (Y, Z), the Y-axis trajectory of the base link of the biped robot is obtained in the same way.

C.2 Asymmetric running

We should not expect to see perfect symmetry in running of biped robots since the control system to provide balanced steady-state behavior should compensate for energy losses due to joint friction, external forces, and uncertainties (Raibert 1986). The biped robot should move asymmetrically in order to maintain stable locomotion, to purposely transit gaits, and to increase power autonomy. Asymmetric running deviates symmetry. Hence, it has difficulty in satisfying repeatability conditions for a steady, asymmetric and repeatable pattern.

For example, the body forms an asymmetric configurations with respect to a vertical axis passing through the hip during a support phase or flight phase. Thus,

$$\begin{aligned} \varphi(0) &= -\gamma_1\varphi(T_s) = \gamma_1\varphi(T_s + T_f), \\ \dot{\varphi}(0) &= \gamma_2\dot{\varphi}(T_s) = \gamma_2\dot{\varphi}(T_s + T_f), \\ l(0) &= \gamma_3 l(T_s) = \gamma_3 l(T_s + T_f), \\ \dot{l}(0) &= -\gamma_4\dot{l}(T_s) = \gamma_4\dot{l}(T_s + T_f) \end{aligned} \tag{68}$$

where parameters γ_1, γ_2, γ_3, and γ_4 are determined by the configuration and speed of the body at touch-down. The body trajectory of the biped robot (X, Z) in the sagittal plane is obtained by inserting $X(t) = l(t)\sin\varphi(t)$, $Z(t) = l(t)\cos\varphi(t)$, and (68) into (64). However, this asymmetric trajectory cannot provide a repeatable pattern for running due to velocity discontinuity at times 0 (touch-down) and $T_s + T_f$ (touch-down).

Asymmetric running should satisfy not only the repeatability condition but also the running stability. In order to meet these necessary conditions, asymmetric behavior of a biped robot including gait transition and change of speed is divided into trajectory segments, and then asymmetric trajectories are constructed using polynomial functions to concatenate these trajectory segments, as given in Sect. 4.

Nomenclature

The subscript 'f' corresponds to the flight phase and the subscript 's' corresponds to the stance phase. And subscripts 'r', 'l', 'b', and 'h' denote the right leg of ρ-joints, left leg of ρ-joints, and upper body of ϱ-joints, the hip link, respectively.

Symbol	Meaning	Defined
O–XYZ	Absolute coordinates	Fig. 1
$H - X_H Y_H Z_H$	Body center coordinates fixed at the body of the robot	Fig. 1
$G - X_G Y_G Z_G$	Mass center coordinates fixed at the mass center of the robot	Fig. 1
$\ddot{\vec{q}}_r, \ddot{\vec{q}}_l \in \Re^\rho$	Joint acceleration of the right and left legs	(1)
$\ddot{\vec{q}}_b \in \Re^\varrho$	Joint acceleration of the upper body	(1)
$\ddot{\vec{x}}_h \in \Re^6$	Actual acceleration of the hip link	(1)
$\dot{\vec{x}}_{h,d}$	Desired acceleration of the hip link	(43)
$\vec{f}_r, \vec{f}_l \in \Re^6$	External force/moment applied at the right and left feet	(1)
$H_r, H_l \in \Re^{\rho\times\rho}$	Inertia matrices of the left and right legs	(1)
$R \in \Re^{6\times6}$	Inertia matrix of the hip link	(1)
$K_r, K_l \in \Re^{\rho\times6}$	Inertia matrices of the left and right legs	(1)
$Q_r, Q_l \in \Re^{6\times\rho}$	Inertia matrices of the hip	(1)
$H_b \in \Re^{\varrho\times\varrho}, K_b \in \Re^{\varrho\times6}$	Inertia matrices of the upper body and the hip link	(1)
$Q_b \in \Re^{6\times\varrho}$	Inertia matrices of the upper body and the hip	(1)
$D, P \in \Re^{6\times6}$	Jacobians of the left and right feet	(1)
$L_r, L_l \in \Re^\rho, L_b \in \Re^\varrho, S \in \Re^6$	Coriolis/centripetal and gravitational forces	(1)
$\vec{\tau}_l, \vec{\tau}_r \in \Re^\rho, \vec{\tau}_b \in \Re^\varrho$	Joint torques of the left leg, right leg and upper body	(1)
I_{gk}	Inertia tensor of k-th link	(2)
$\vec{\omega}_{gk}$	Angular velocity of k-th link with respect to the absolute coordinates	(2)
$\vec{x}_h^0$	Linear velocity of the hip link with respect to the absolute coordinates	(2)
$\vec{\omega}_h^0$	Angular velocity of the hip link with respect to the absolute coordinates	(2)
$\vec{P}_0$	Linear momentum represented by the absolute coordinates	(2)
$\vec{H}_0$	Angular momentum represented by the absolute coordinates	(2)
$\vec{P}_G = [(\vec{P}_G)_x\ (\vec{P}_G)_y\ (\vec{P}_G)_z]^T$	Linear momentum at the mass center of the robot	(3)
$\vec{H}_G = [(\vec{H}_G)_x\ (\vec{H}_G)_y\ (\vec{H}_G)_z]^T$	Angular momentum at the mass center of the robot	(4)
$\vec{r}_g = [X_g\ Y_g\ Z_g]^T$	Position vector of the center of mass	(4)
$\vec{r}_h = [X\ Y\ Z]^T$	Position vector of the hip link	(56)
m_g	Total mass of a biped robot	(4)
m_k	Mass of k-th link	(3)
$\vec{r}_k = [x_k\ y_k\ z_k]^T$	Position vector of k-th link represented by the absolute coordinates	(3)
J_{kx}, J_{ky}, J_{kz}	Inertia moments of k-th link about the mass center coordinates	(4)
$\dot{\phi}_{kx}, \dot{\phi}_{ky}, \dot{\phi}_{kz}$	Angular velocities of k-th link about the mass center coordinates	(4)
$\dot{\vec{H}}_{Ok}$	Rate of change in angular momentum of k-th link	(6)
$\dot{\vec{H}}_{Gk}$	Rate of change in angular momentum of k-th link about the mass center	(6)
$\ddot{\vec{r}}_k$	Acceleration of the center of mass of k-th link about the absolute coordinates	(6)
$\vec{g} = [0\ 0\ -g]^T$	Gravitational acceleration	(6)
$X_{\rm zmp}, Y_{\rm zmp}$	x-component and y-component of the ZMP	(10)
l_h	Length from the center of the foot to the rear safety boundary	(10)
l_t	Length from the center of the foot to the fore safety boundary	(10)
$(\vec{H}_G)_{y,td+}$	Angular momentum at the moment $t = t_{td+}$ after touch-down	(13)
$(\vec{H}_G)_{y,td-}$	Angular momentum at the moment $t = t_{td-}$ before touch-down	(13)
$\alpha_0, \alpha_1, \alpha_2, \alpha_3$	Positive values which is determined by support phase trajectories	(14)
β_1, β_2	Positive values which is determined by support phase trajectories	(17)
V_{xf}, V_{yf}, V_{zf}	Desired velocity of the hip link at lift-off	Fig. 3
$\dot{X}_C, \dot{Y}_C, \dot{Z}_C$	Desired velocity of the hip link at touch-down in the running model	Fig. 3
$\dot{X}_{C,td}, \dot{Y}_{C,td}, \dot{Z}_{C,td}$	Actual velocity of the hip link at touch-down	Fig. 3
M	Total mass of the trunk and upper parts of the robot	Fig. 3
M_1	Mass concentrated at the middle of the left leg	Fig. 3
M_2	Mass concentrated at the middle of the right leg	Fig. 3
$(\vec{P}'_G)_x,\ (\vec{P}'_G)_y,\ (\vec{P}'_G)_z$	Modified components of linear momentum	(18)

Symbol	Meaning	Defined
$(X_j,\ Y_j,\ Z_j)$	Position of the hip link of each breakpoint in the running model	Fig. 3
$(X_{ij},\ Y_{ij},\ Z_{ij})$	Foot position of each breakpoint in the running model	Fig. 3
T_f	Duration of the flight phase	(18)
$(\overline{X}_j,\ \overline{Y}_j,\ \overline{Z}_j)$	Center of mass of the running model	(19)
$\dot{\overline{X}}_{lo},\ \dot{\overline{Y}}_{lo},\ \dot{\overline{Z}}_{lo}$	Initial velocities of the model's center of mass	(19)
$\dot{X}_A,\ \dot{Y}_A,\ \dot{Z}_A$	Initial position of the hip link in the running model	Fig. 3
σ	Value which arises from insisting on continuous acceleration lift-off	(20)
l_0	Nominal length which is the leg length at touch-down and lift-off	Fig. 4
l	Leg length at any time	Fig. 4
φ	Angle with the vertical axis in the sagittal plane	Fig. 4
ψ	Angle with the vertical axis in the frontal plane	Fig. 4
T_s	Duration of a support phase	Fig. 5
k_{leg}	Stiffness of a supporting leg	Fig. 5
H_z	Vertical height of the hip link at touch-down and lift-off	Fig. 5
S_t	Stride of a support phase	Fig. 5
$H_{z,min}$	Lower limit of H_z to avoid the collision between links	Sect. 4.2
$H_{z,max}$	Upper limit of H_z to avoid the singular configuration	Sect. 4.2
$S_{t,min}$	Lower limit of S_t determined by the desired forward velocity of the robot	Sect. 4.2
$[X_{CA},\ \dot{X}_{CA}]$	Configuration and speed of the hip link in the middle of the support phase	(29)
$[X_{sf},\ Y_{sf},\ Z_{sf}]$	Position of a swing foot during the support phase	(32)
$Z_{1C,td}$	Actual vertical position of a swing foot at touch-down	(32)
$f_h \in \Re^1$	Tangential component of the external force generated by the ground	(33)
$f_v \in \Re^1$	Normal component of the external force generated by the ground	(33)
$f_{v,d} \in \Re^1$	Normal component of the external force generated by the ground	(50)
$\vec{f}_{l,d}$	Desired external force vector applied at the left foot	(51)
μ_s, μ_d	Static coefficient and dynamic coefficient of friction	(33), (34)
θ	Angle between the foot's force f_t and the normal force f_v	(34)
$\dot{\vec{x}}_{lf} \in \Re^6$	Velocity of the left foot about O	(36)
$\dot{\vec{x}}_{rf} \in \Re^6$	Actual velocity of the right foot represented by the absolute coordinates	(47)
$\dot{\vec{x}}_{rf,d} \in \Re^6$	Desired velocity of the right foot represented by the absolute coordinates	(47)
$R_h^0 \in \Re^{3\times3}$	Orientation matrix of the body center coordinate system	(36)
$\dot{\vec{x}}_{lf}^0 \in \Re^3, \vec{\omega}_{lf}^0 \in \Re^3$	Linear velocity and angular velocity of the left foot	(36)
$J_l \in \Re^{6\times6}$	Jacobian matrix of the left foot with respect to the hip	(37)
$J_r \in \Re^{6\times6}$	Jacobian matrix of the right foot with respect to the hip	(37)
$\dot{\vec{x}}_{lf}^h \in \Re^6$	Velocity vector of the left foot with respect to the hip	(37)
(M_L, D_L, E_L)	Desired mass, damping, and stiffness matrices about the left leg	(38)
M_h, D_h, E_h	Desired mass, damping ratio and stiffness matrices about the hip link	(43)
M_R, D_R, E_R	Desired mass, damping ratio and stiffness about the rear right leg	(47)
$\Delta f, \delta$	Reduction rate and boundary value for force modulation	(50)
V_k	Armature voltage of k-th revolute joint	(52)
i_k	Armature current of k-th revolute joint	(52)
η	Gear reduction ratio	(52)
j_m	Sum of the DC motor and gear train inertias	(52)
b_m	Sum of viscous-friction coefficients of the DC motor and gear	(52)
k_T	Torque constant of the motor	(52)
k_b	Back electro-motive force constant of the motor	(52)
r_a	Armature resistance of the motor	(52)
i_{max}, V_{max}	Maximum current, maximum voltage	(52)
F_x, F_y, F_z	External forces generating at the supporting foot	(55)
I_{kx}, I_{ky}, I_{kz}	Inertia moments of k-th link represented by the absolute coordinates	(54)

References

Ahmadi, M., & Buehler, M. (1997). Stable control of a simulated one-legged running robot with hip and leg compliance. *IEEE Transactions on Robotics and Automation*, *13*(1), 96–104.

Alexander, R. M. (1990). Three uses for springs in legged locomotion. *International Journal of Robotics Research*, *9*(2), 53–61.

Arikawa, K., & Mita, T. (2002). Design of multi-DOF jumping robot. In *IEEE int. conf. on robotics and automation* (pp. 3992–3997).

Boone, G. N., & Hodgins, J. K. (1997). Slipping and tripping reflexes for bipedal robots. *Autonomous Robots*, *4*, 259–271.

Cavagna, G. A., Thys, H., & Zamboni, A. (1976). The source of external work in level walking and running. *Journal of Physiology*, *262*, 639–657.

Chevalereau, C., Westervelt, E. R., & Grizzle, J. W. (2005). Asymptotically stable running for a five-link, four-actuator, planar bipedal robot. *International Journal of Robotics Research*, *24*(6), 431–464.

Erbatur, K., Okazaki, A., Obiya, K., Takahashi, T., & Kawamura, A. (2002). A study on the zero moment point measurement for biped walking robots. In *Int. workshop on advanced motion control* (pp. 431–436).

Francois, C., & Samson, C. (1998). A new approach to the control of the planar one-legged hopper. *International Journal of Robotics Research*, *17*(11), 1150–1166.

Frohlich, C. (1979). Do springboard divers violate angular momentum conservation?. *American Journal of Physics*, *47*, 583–592.

Fujimoto, Y., & Kawamura, A. (1998). Simulation of an autonomous biped walking robot including environmental force interation. *IEEE Robotics and Automation Magazine*, *5*(2), 33–42.

Hodgins, J. K. (1991). Biped gait transitions. In *IEEE int. conf. on robotics and automation* (pp. 2092–2097).

Hodgins, J. K., & Raibert, M. H. (1991). Adjusting step length for rough terrain locomotion. *IEEE Transactions on Robotics and Automation*, *7*(3), 289–298.

Hyon, S., & Emura, T. (2004). Running control of a planar biped robot based on energy-preserving strategy. In *IEEE int. conf. on robotics and automation* (pp. 3791–3796).

Ikeda, T., Iwatani, Y., Suse, K., & Mita, T. (1999). Analysis and design of running robots in touchdown phase. In *IEEE int. conf. on control applications* (pp. 22–27).

Kajita, S., Nagasaki, T., Yokoi, K., Kaneko, K., & Tanie, K. (2002). Running pattern generation for a humanoid robot. In *IEEE int. conf. on robotics and automation* (pp. 2755–2761).

Kajita, S., Nagasaki, T., Kaneko, K., Yokoi, K., & Tanie, K. (2004). A hop towards running humanoid biped. In *IEEE int. conf. on robotics and automation* (pp. 629–635).

Kajita, S., Nagasaki, T., Kaneko, K., Yokoi, K., & Tanie, K. (2005). Running controller of humanoid biped HRP-2LR. In *IEEE int. conf. on robotics and automation* (pp. 616–622).

Kwon, O., & Park, J. H. (2002). Locomotion control of biped robot on a slippery surface using reflex control. *Advanced Robotics*, *16*(8), 721–734.

Kwon, O., & Park, J. H. (2003). Gait transitions for walking and running of biped robot. In *IEEE int. conf. on robotics and automation* (pp. 1350–1355).

Lapshin, V. V. (1991). Motion control of a legged machine in the supportless phase of hopping. *International Journal of Robotics Research*, *10*(4), 327–337.

Lewis, F. L., Abdallah, C. T., & Dawson, D. M. (1993). *Control of robot manipulators*. Englewood Cliffs: Prentice-Hall.

Li, Q., Takanishi, A., & Kato, I. (1991). A biped walking robot having a zmp measurement system using universal force-moment sensors. In *IEEE/RSJ int. workshop on intelligent robots and systems* (pp. 1568–1573).

Marhefka, D. W., & Orin, D. E. (1999). A compliant contact model with nonlinear damping for simulation of robotic systems. *IEEE Transactions on Systems, Man, and Cybernetics–Part A: Systems and Humans*, *29*(6), 566–572.

McMahon, T. A. (1984). *Muscles, reflexes, and locomotion*. Princeton: Princeton University Press.

Nagasaka, K., Kuroki, Y., Suzuki, S., Itoh, Y., & Yamaguchi, J. (2004). Integrated motion control for walking, jumping and running on a small bipedal entertainment robot. In *IEEE int. conf. on robotics and automation* (pp. 3189–3194).

Nagasaki, T., Kajita, S., Yokoi, K., Kaneko, K., & Tanie, K. (2003). Running pattern generation and its evaluation using a realistic humanoid model. In *IEEE int. conf. on robotics and automation* (pp. 1336–1342).

Nunez, V., & Nadjar-Gauthier, N. (2005). Humanoid vertical jump with compliant contact. In *Int. conf. on climbing and walking robots* (pp. 457–464).

Oh, S. Y., & Orin, D. (1986). Dynamic computer simulation of multiple closed-chain robotic mechanisms. In *IEEE int. conf. on robotics and automation* (pp. 15–20).

Papadopoulos, E., & Cherouvim, N. (2004). On increasing energy autonomy for one-legged hopping robot. In *IEEE int. conf. on robotics and automation* (pp. 4645–4650).

Park, J. H. (2001). Impedance control of biped locomotion. *IEEE Transactions on Robotics and Automation*, *17*(6), 870–882.

Park, J. H., & Kim, K. D. (1998). Biped robot walking using gravity-compensated inverted pendulum mode and computed torque control. In *IEEE int. conf. on robotics and automation* (pp. 3528–3533).

Park, J. H., & Kwon, O. (2003). Impedance control for running of biped robots. In *IEEE/ASME int. conf. on advanced intelligent mechatronics*.

Playter, R. R., & Raibert, M. H. (1992). Control of a biped somersault in 3d. In *IEEE int. conf. on intelligent robots and systems* (pp. 582–589).

Raibert, M. H. (1986). *Legged robots that balance*. Cambridge: MIT Press.

Ramachandra, K. V. (2000). *Kalman filtering techniques for radar tracking*. New York: Dekker.

Ramey, M. R. (1973). Significance of angular momentum in long jumping. *The Research Quarterly of the American Association for Health, Physical Education, and Recreation*, *44*(4), 488–497.

Saranli, U., Schwind, W. J., & Koditschek, D. E. (1998). Toward the control of a multi-jointed, monopod runner. In *IEEE int. conf. on robotics and automation* (pp. 2767–2682).

Seyfarth, A., Geyer, H., Günther, M., & Blickhan, R. (2002). A movement criterion for running. *Journal of Biomechanics*, *35*, 649–655.

Spong, M. W., & Vidyasagar, M. (1989). *Robot dynamics and control*. New York: Wiley.

Thorstensson, A., & Roberthson, H. (1987). Adaptations to changing speed in human locomotion: speed of transition between walking and running. *Acta Physiol Scand*, *131*, 211–214.

Vukobratovic, M., & Juricic, D. (1969). Contribution to the synthesis of biped gait. *IEEE Transactions on Bio-Medical Engineering*, *BME-16*(1), 1–6.

Walker, M. W., & Orin, D. E. (1982). Efficient dynamic computer simulation of robotic mechanisms. *ASME Journal of Dynamic Systems, Measurement and Control*, *104*, 205–211.

Yamaguchi, J., Takanishi, A., & Kato, I. (1995). Experimental development of a foot mechanism with shock absorbing material for acquisition of landing surface position information and stabilization of dynamic biped walking. In *IEEE int. conf. on robotics and automation* (pp. 2892–2899).

Ohung Kwon received the B.S. degree in the School of Mechanical Engineering and the M.S. degree in the Department of Precision Mechanical Engineering from Hanyang University, Seoul, Korea, in 1999 and 2001, respectively. He is currently a Ph.D. student in the Department of Mechanical Engineering, Hanyang University, Seoul, Korea. His current research interests are related to biped/quadruped robots, SLAM, and virtual reality.

Jong Hyeon Park received the B.S. degree in mechanical engineering from Seoul National University, Seoul, Korea, in 1981 and the S.M. and Ph.D. degrees from the Massachusetts Institute of Technology (MIT), Cambridge, in 1983 and 1991, respectively. Since 1992, he has been with the School of Mechanical Engineering at Hanyang University, Seoul, Korea, where he is currently a Professor. He was a KOSEF (Korea Science and Engineering Foundation)–JSPS (Japan Society for the Promotion of Science) Visiting Researcher with Waseda University, Tokyo, Japan, in 1999, and a KOSEF-CNR (Consiglio Nazionale delle Ricerche) Visiting Researcher with Scuola Superiore Sant'Anna, Pisa, Italy, in 2000, a Visiting Scholar with MIT, Cambridge, USA, in 2002–2003. He was also associated with Brooks Automation Inc., Chelmsford, MA, in 1991–1992 and 2001–2002. His research interests include biped robots, robot dynamics and control, haptics, and bio-robots. He is a member of the IEEE (Institute of Electrical and Electronics Engineers), KSME (Korea Society of Mechanical Engineers), ICROS (Institute of Control, Robotics and Systems), KROS (Korea Robotics Society), KSAE (Korean Society of Automotive Engineers), KSPE (Korean Society of Precision Engineering) and KSEE (Korean Society for Engineering Education).